ectoderm protein (**a**, GFAP; **e**, βIII-tubulin), mesoderm protein (**b**, SMA), and endoderm (**f**, AFP) protein on hiPSCs (HPS0077) after culture on PVA-24h-1000 dishes under xeno-free conditions for 20 passages. (**c**) Hoechest staining of hESCs used in (**a**,**b**). (**d**) Merged picture of (**a**–**c**). (**g**) Hoechest staining of hESCs used in (**e**,**f**). (**h**) Merged picture of (**e**–**g**). The bar indicates 100 μm.

No completely synthetic polymer substrates are commercially available for hPSC culture. Therefore, it is necessary to investigate whether hPSCs can be cultured on completely synthetic polymer substrates with high reproducibility by different groups of researchers if these substrates will be used for hPSC cultures in the future.

The PVA-24h-1000 dishes developed in this study contained the hPSC binding domain of oligoVN, which binds to integrins $\alpha_V\beta_3$ and $\alpha_V\beta_5$[8]. Therefore, hESCs cultured on MEFs can be directly shifted onto PVA-24h-1000 dishes without any differentiation, whereas hESCs cultured on Synthemax II dishes exhibit significant differentiation (Fig. 5), although the binding site of hPSCs on Synthemax II dishes is reported to be the same amino acid sequence to oligoVN used in PVA-oligoVN dishes in this study[25].

The effect of the elasticity of cell culture matrices on stem cell fate in terms of pluripotency and differentiation has been primarily investigated for adult stem cells, such as mesenchymal stem cells and hematopoietic stem cells[46–48]. However, in this study we found that fine-tuning the elasticity of hPSC culture matrices was very important for the attachment and expansion of hPSCs. Only a few small or no hPSC colonies were observed on the softest substrates (10–20 kPa), whereas hPSCs cultured on the stiffest substrates (e.g., storage modulus of 30 kPa) tended to differentiate after five days of culture. hPSCs cultured on the optimal elastic substrates (25 kPa) maintained their pluripotency for more than 20 passages under xeno-free and feeder-free conditions. The culture of hSPCs on Synthemax II dishes for 20 passages under xeno-free and feeder-free conditions has been reported in the literature[25]. However, hPSCs tended to more easily differentiate on the Synthemax II dishes compared to hPSCs cultured on Matrigel and the PVA-24h-1000 dishes developed in this study. This result is because the base cell culture dishes of Synthemax II are stiff TCPS with an approximately 12 GPa modulus[48], which is too stiff a surface for hPSC culture. If Synthemax II is coated on the softer hydrogels, the differentiation ability of hPSCs might decrease and the Synthemax II dishes would be more adequate for hPSC culture.

Matrigel-coated dishes supported long-term expansion of hPSCs maintaining their pluripotency. Matrigels are known to contain variety of ECMs as well as growth factors, which support long-term culture of hPSCs maintaing their pluripotency. Although Matrigels were coated on stiff TCPS, matrigel layer on TCPS may contribute to generate somewhat soft cell culture biomaterials (less stiffness compared to solely TCPS surface) for hPSCs that can be cultured for long-term and keep their pluripotency on Matrigel-coated dishes.

Musah *et al.* cultured hESCs on glycosaminoglycan-binding acrylamide hydrogels with 0.7 kPa, 3 kPa, and 10 kPa[33]. They found only relatively stiff hydrogels (10 kPa) could maintain hESC proliferation, which is similar to our results demonstrating that extremely soft hydrogels (0.7–3 kPa) cannot attach and maintain hESCs. Unfortunately, this study did not report hESC proliferation on hydrogels with a surface stiffer than 10 kPa, because the present study found that the optimal elasticity of the hydrogels was 25 kPa. However, their study indicates that hESCs can respond to mechanical information from cell culture matrices via glycosaminoglycan engagement, which can be fine-tuned to activate specific signaling pathways linked to pluripotency.

Chang *et al.* developed hydrogels containing heparin-mimicking moieties, which have different bulk modulus by varing their crosslinking density (54, 138, and 344 kPa)[55]. Their hydrogels with low bulk elasticity (54 kPa) supported minimal cell adhesion of hESCs and those having a moderate elasticity of 138 kPa demonstrated some cell adhesion of hESCs, but the attached cells exhibited spontaneous differentiation. They found the most rigid hydrogels in their study (344 kPa) exhibited good attachment of hESCs and supported long-term expansion of hESCs maintaining their pluripotency for >20 passages. Their hydrogels do not have direct binding site of hESCs, but have FGF-2 binding site due to the existence of heparin-mimicking moieties, which contribute to the binding of hESCs. Especially, their softer hydrogels have less binding of FGF-2 due to lower density of heparin-mimicking moieties. Therefore, their hydrogel needs minimum rigidity to attach hESCs, which contributes to the existence of the threshold amount of FGF-2 binding site (hESCs binding site) in their hydrogels. In our study, PVA-24h-1000 hydrogels having 25 kPa storage modulus are the best biomaterials to support long-term expansion of hPSCs maintaining their pluripotency. Both Chang's work and present study demonstrated that there is the optimal elasticity of the hydrogels that can support long-term expansion of hPSCs. The difference of optimal elasticity among Chang's work and present study to support long-term expansion of hESCs should be originated from different design of base materials of hydrogels.

Important considerations for the design of biomaterials for hPSC cultures include the optimization of the elasticity (physical cues) of the biomaterials and the selection and fine-tuning of the surface density of bioactive cell-binding nanosegments (biological cues) on the surface of the biomaterials. PVA-IA hydrogels with an optimal elasticity of 25 kPa and oligoVN concentrations greater than 500 μg/ml were selected in this study for optimal hPSC culture. The PVA-24h-500, PVA-24h-1000, and PVA-24h-1500 dishes showed higher attachment ratios and lower differentiation ratios of hPSCs compared to the commercially available Synthemax II dishes. This is because Synthemax II dishes are prepared by coating a bioactive polymer on conventional stiff tissue culture dishes; therefore, Synthemax II dishes do not have the optimal elasticity for the culture of hPSCs, whereas the PVA-oligoVN dishes developed in this study have optimized elasticity for hPSC culture due to the control of the crosslinking density of the PVA-IA hydrogels. hPSCs can be cultured on PVA-24h-1000 dishes for long-term passage (i.e., 20 passages) by maintaining their pluripotency and ability to differentiate into cells derived from the three germ layers both *in vitro* and *in vivo*.

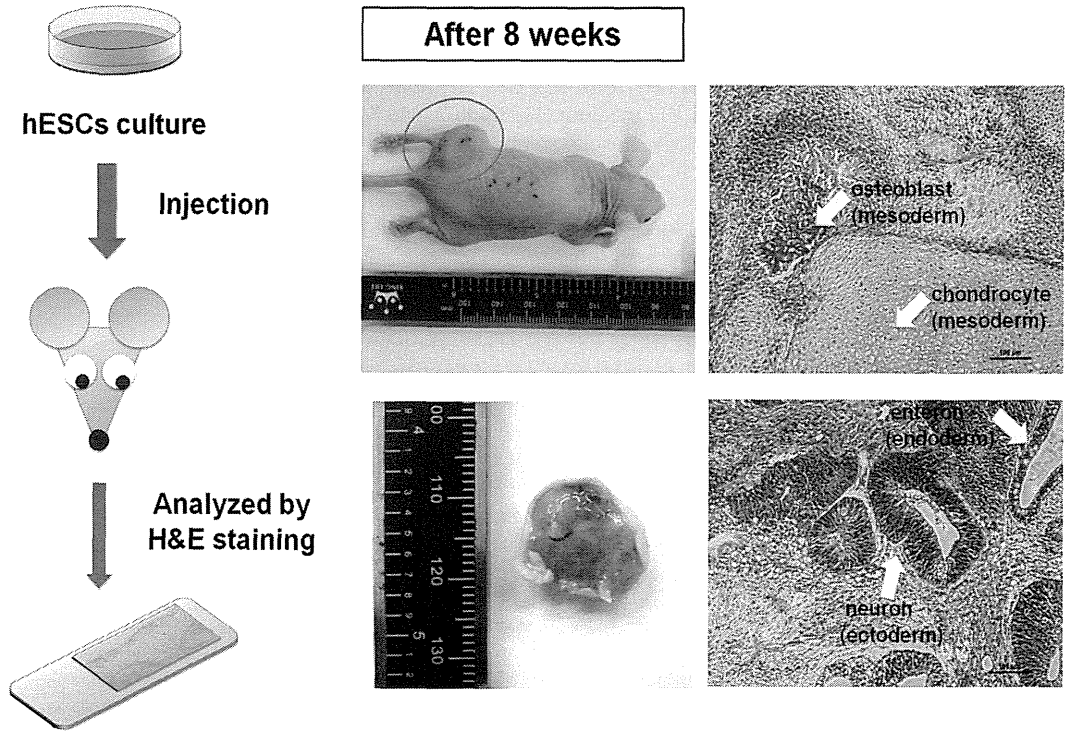

Figure 8. Characterization of the differentiation ability of hPSCs (hESCs and hiPSCs) *in vivo* after culture on PVA-oligoVN hydrogels for 20 passages. Pluripotency of teratoma-forming hESCs (WA09) after culture on PVA-24h-1000 dishes under xeno-free conditions for 20 passages. Osteoblasts and chondrocytes (mesoderm), neurons (ectoderm), and enterons (endoderm) can be detected. The bar indicates 100 μm.

(a)	Coating materials of ECMs
	Gelatin[19], fibronectin[23], laminin[18], **laminin-332**[11], **laminin-511**[12], **laminin-521**[13], **vitronectin**[15], **recombinant vitronectin**[14]
(b)	Polysaccharide substrates
	Chitin/alginate, cellulose, positively charged cellulose
(c)	Oligopeptides for immobilization on substrates
	Poly-D-lysine, cyclicRGD[27], pronectin[28], **oligovitronectin**[25,26]
(d)	Chimera protein for immobilization on substrates
	E-cadherin chimera[53]
(e)	Synthetic polymer of substrates[b]
	MEASAH, PMVE-alt-MA[39], PMEDSAH[40–43], APMAAm[44],Copoly(AEtMA-co-DEAEA)[45], Poly-3,4-dihydroxy-L-phenyl-alanine

Table 1. Coating and substrates for feeder-free hPSC culture in a defined medium[a]. [a]Bold biomolecules are typically used. [b]PMVE-alt-MA, poly(methyl vinyl ether-alt-maleic anhydride); PMEDSAH, poly[2-(methacryloyloxy(ethyl dimethyl-(3-sulfopropyl)ammoniumhydroxide; APMAAm, aminopropylmethacrylamide; Copoly(AEtMA-co-DEAEA), copoly[2-(acryloyloxyethyl) trimethylammonium-co-2-(diethylamino)ethyl acrylate].

Conclusion

We have developed PVA-oligoVN hydrogels having different elasticity for long-term expansion of hPSCs maintaining their pluripotency for 20 passages. The optimal elasticity of cell culture biomaterials is necessary to maintain pluripotency (e.g., 25.3 kPa) when hPSCs are cultured on PVA-oligoVN hydrogels. It is also necessary to use high concentration of oligoVN (500–1500 μg/ml) for the preparation of PVA-oligoVN hydrogels to maintain the pluripotency. The optimization of the elasticity (physical cues) of the biomaterials as well as the selection and fine-tuning of the surface density of bioactive cell-binding nanosegments (biological cues) on the surface of the biomaterials is important for the design of biomaterials for long-term expansion of hPSCs maintaining their pluripotency.

Materials and methods

Materials. hESCs (WA09) were obtained from the WiCell Research Institute, Inc (Madison, WI, USA). hiPSCs (HPS0077) were obtained from the Riken BioResource Center (Tsukuba, Japan). Corning Synthemax II-SC

(3535XX1) was purchased from Sigma-Aldrich (St. Louis, MO, USA). Matrigel (354230, growth factor-reduced basement membrane matrix) was obtained from BD Biosciences (San Jose, CA, USA). mTeSR1 medium (05850) was obtained from Stem Cell Technologies. Essential 8 medium (A1517001), Essential 6 medium (A1516401), DMEM/F12 medium (11330-057), and KnockOut Serum Replacement (10828-028) were purchased from Life Technology. The oligopeptide of oligoVN (KGGPQVTRGDVFTMP) was obtained from PHJapan (Hiroshima, Japan). TCPS dishes (diameter = 35 mm, 35-3001) were purchased from Becton Dickinson (Franklin Lakes, NJ, USA). N-(3-Dimethylaminopropyl)-N'-ethylcarbodiimide hydrochloride (EDC, 03450), N-hydroxysuccinimide (NHS, 13062), and glutaraldehyde (25% in water, G5882) were obtained from Sigma-Aldrich (St. Louis, MO, USA). The antibody against Oct3/4 (anti-octamer-binding transcription factor 3/4 IgG, sc-5279, mouse) was obtained from Santa Cruz Biotechnology (Dallas, TX, USA). The antibody against Sox2 (anti-SRY (sex determining region Y)-box 2 IgG, ab5603, rabbit) and the alkaliphosphatase detection kit (SCR004) were obtained from EMD Millipore (Billerica, MA, USA). The antibodies against SSEA-4 (anti-stage-specific embryonic antigen-4 IgG, ab16287, mouse) and TRA-1-81 (anti-tumor rejection antigen-1-81 IgG, ab16289, mouse) were purchased from Abcam (Cambridge, MA, USA). The antibodies against GFAP (anti-glial fibrillary acidic protein IgG, MA5-15086, mouse), AFP (anti-alpha-fetoprotein IgG, PA5-21004, mouse), SMA (anti-smooth muscle actin IgG, PA5-19465, rabbit), Alexa Fluor 488 goat anti-mouse IgG (H + L) (A11001), Alexa Fluor 488 goat anti-rabbit IgG (H + L) (A11008), and Alexa Fluor 594 donkey anti-rabbit IgG (H + L) (A21207) were purchased from Life Technology (Carlsbad, CA, USA). The antibody against βIII-Tubulin (MCA2047, mouse) was obtained from AbD Serotec (Raleigh, NC, USA). Hoechst 33342 (PA-3014) was obtained from Lonza (Basel, Switzerland). The other chemicals employed were reagent grade and were used without further purification; these chemicals were purchased from Sigma-Aldrich (St. Louis, MO, USA). Ultrapure water produced by a Milli-Q system (Millipore Corporation, Billerica, MA, USA) was used throughout the experiments.

Preparation of crosslinked PVA-IA hydrogel dishes. PVA-IA (Japan VAM & Poval Co., Ltd., Osaka, Japan) with 1.3 mol% itaconic acid showing a degree of hydrolysis of 97.7% and a degree of polymerization of 1750 was dissolved to 0.05 wt% for the cell culture experiments or 0.5 wt% for the rheometer measurements in ultrapure water. Then, the solutions were agitated for two days and subsequently kept at room temperature for one day to ensure that no air bubbles were present[48]. A 3 mL aliquot of the PVA-IA solution was added to a 35 mm TCPS dish and dried for a week on a clean bench to produce a film. The PVA-IA films were immersed in an aqueous crosslinking solution composed of 1 wt% glutaraldehyde, 20 wt% sodium sulfate, and 1 wt% sulfuric acid for 0.5, 1, 6, 24, and 48 h (Fig. 1). The naming convention 'PVA-*X*' (e.g., PVA-24h) indicates PVA-IA hydrogels crosslinked for *X* hours (e.g., 24 h). After crosslinking, the PVA-IA hydrogels were washed with ultrapure water and then immersed in ultrapure water. The ultrapure water was changed twice daily prior to grafting with oligoVN and use in cell culture. The PVA-IA hydrogels were sterilized via immersion in a 75 v/v% ethanol solution overnight, washed in ultrapure water and kept in ultrapure water until use for cell culture.

Preparation of PVA-IA hydrogel dishes grafted with oligoVN. Following the preparation of PVA-IA hydrogels with different elasticities, the hydrogels were activated via immersion in an aqueous solution containing 10 mg/ml EDC and 10 mg/ml NHS for 6 h at 25 °C. Subsequently, the PVA-IA hydrogels were washed with phosphate buffered saline (PBS, pH7.2) and immersed in a PBS solution containing 100–1500 μg/mL of oligoVN for 24 h at 4 °C (Fig. 1). After grafting oligoVN, the PVA-IA hydrogels were washed with ultrapure water for 12 h to remove residual oligoVN. The PVA-IA hydrogels grafted with *Y* μg/mL of oligoVN are hereafter referred to as PVA-*X*h-*Y*, where *X* indicates the crosslinking time (h).

Characterization of PVA-IA hydrogel dishes grafted with oligoVN. The chemical composition of the surface-grafted PVA-IA hydrogel dishes was measured using X-ray photoelectron spectroscopy (XPS, K-Alpha spectrometer, Thermal Scientific, Inc., Amarillo, TX, USA, equipped with a monochromatic Al-K X-ray source [1,486.6 eV photons]). The energy of the emitted electrons was measured using a hemispherical energy analyzer at pass energies ranging from 50 to 150 eV. Data were collected at a photoelectron takeoff angle of 45 degrees with respect to the sample surface. The binding energy (BE) scale was referenced by setting the peak maximum in the C1s spectrum to 284.6 eV. The obtained high-resolution C1s spectra were fitted using Shirley background subtraction and a series of Gaussian peaks.

The storage modulus of the PVA-IA hydrogels prepared from a 5 wt% PVA-IA solution and crosslinked for 0.5–48 h were quantified using a rheometer (Physica MCR 101, Anton Pars Co. Ltd.) with a 5% strain at 1 Hz.

hPSC culture. The hESC line WA09 (H9) was maintained as previously described on mitomycin-C-treated mouse embryonic fibroblast (MEF) feeder cells in DEME/F12 medium supplemented with 20% KnockOut Serum Replacement[56]. WA09 cells were split into two lines: one group of WA09 cells was maintained on MEFs and the other group was maintained on Matrigel as previously described[42]. The hiPSC line HS0077 was maintained on Matrigel in Essential 8 medium. Experimental control cells were obtained from conventional colony cultures and maintained as previously described[11]. Briefly, near-confluent cells were incubated with 2 mg/ml dispase in DMEM/F-12 medium at 37 °C for 2 min and then rinsed twice with DMEM/F12 medium. After addition of DMEM/F-12 medium, weakly adherent colonies were detached using a cell scraper. Cells were collected and centrifuged at 160 × g for 5 min at 37 °C. Small colonies were passaged into Matrigel-coated dishes or MEFs at a 1:4 ratio. Colonies showing morphological differentiation were manually removed under a microscope during each passage except at the time of analysis. Completely dissociated cells were cultured after preculture in the appropriate defined medium (mTeSR1 or Essential 8) for nine passages on Matrigel-coated dishes to remove MEF feeders. This stage was defined as passage 0. Near-confluent cell clusters were treated with dispase for 1–2 min at 37 °C. Cells in defined medium were pipetted to disperse the cells completely. After centrifugation at 160 × g for 5 min at 4 °C,

the cells were seeded at the appropriate density ($5x10^4$ cells per cm^2 for passaging or as indicated) into new culture dishes (PVA-IA hydrogels grafted with oligoVN). The medium was changed daily for all experiments.

hPSC characterization. The alkaline phosphatase (AP) activity of hiPSCs was measured using an alkaline phosphatase detection kit according to the manufacturer's instructions[26].

Immunostaining of Oct3/4, Sox2, SSEA-4, and Tra-1-81 was performed on hPSCs to evaluate pluripotency following the conventional protocol[26]. The stained cells were analyzed using fluorescence microscopy (Eclipse Ti-U fluorescence inverted microscope, Nikon Instruments, Inc., Tokyo, Japan).

Embryoid body formation. hPSC pluripotency was evaluated by embryoid body (EB) formation at passages 10 and 20. hPSCs were dissociated from the substrate as described above for passages. Cells in the supernatant were collected, counted using a hemocytometer, and seeded onto ultra-low attachment dishes in Essential 6 medium to form EBs. After 2 weeks in suspension, EBs were transferred to Matrigel-coated dishes and cultured in Eseential 6 medium for an additional 3–5 weeks. Then, the cells were stained with antibodies against markers of all three embryonic germline layers (AFP, GFAP, βIII-Tubulin, and SMA) and analyzed by the immunofluorescence method[19].

Teratoma formation. The experiments in this study were approved by the ethics committees of the National Central University and the Taiwan Landseed Hospital (IRB-13-05). All experiments were performed in accordance with all applicable and relevant institutional and governmental regulations and guidelines during this study. Cells were harvested by treatment with a non-enzymatic cell dissociation solution. After centrifugation, the pellets were suspended in DMEM/F12-Matrigel. In total, 5×10^6 cells were injected subcutaneously into SCID mice (6–8 weeks). After 6–8 weeks, teratomas were dissected and fixed with formaldehyde solution. Paraffin-embedded teratomas were sectioned and stained with hematoxylin and eosin[19].

Statistical analysis. All of the quantitative results were obtained from four samples. The data are expressed as the mean ± SD. Statistical analyses were performed using the unpaired Student's *t*-test in Excel (Microsoft Corporation). Probability values (p) less than 0.05 were considered statistically significant.

References

1. Thomson, J. A. *et al.* Embryonic stem cell lines derived from human blastocysts. *Science* **282,** 1145–1147 (1998).
2. Takahashi, K. *et al.* Induction of pluripotent stem cells from adult human fibroblasts by defined factors. *Cell* **131,** 861–872 (2007).
3. Yu, J. *et al.* Induced pluripotent stem cell lines derived from human somatic cells. *Science* **318,** 1917–1920 (2007).
4. Pagliuca, F. W. *et al.* Generation of functional human pancreatic beta cells *in vitro*. *Cell* **159,** 428–439 (2014).
5. Rezania, A. *et al.* Reversal of diabetes with insulin-producing cells derived *in vitro* from human pluripotent stem cells. *Nat. Biotechnol.* **32,** 1121–1133 (2014).
6. Kriks, S. *et al.* Dopamine neurons derived from human ES cells efficiently engraft in animal models of Parkinson's disease. *Nature* **480,** 547–551 (2011).
7. Higuchi, A., Ling, Q. D., Ko, Y. A., Chang, Y. & Umezawa, A. Biomaterials for the feeder-free culture of human embryonic stem cells and induced pluripotent stem cells. *Chem. Rev.* **111,** 3021–3035 (2011).
8. Higuchi, A. *et al.* Design of polymeric materials for culturing human pluripotent stem cells: Progress toward feeder-free and xeno-free culturing. *Prog. Polym. Sci.* **39,** 1348–1374 (2014).
9. Chen, G. *et al.* Chemically defined conditions for human iPSC derivation and culture. *Nat. Methods* **8,** 424–429 (2011).
10. Tsutsui, H. *et al.* An optimized small molecule inhibitor cocktail supports long-term maintenance of human embryonic stem cells. *Nat. Commun.* **2,** 167 (2011).
11. Miyazaki, T. *et al.* Laminin E8 fragments support efficient adhesion and expansion of dissociated human pluripotent stem cells. *Nat. Commun.* **3,** 1236 (2012).
12. Rodin, S. *et al.* Long-term self-renewal of human pluripotent stem cells on human recombinant laminin-511. *Nat. Biotechnol.* **28,** 611–615 (2010).
13. Rodin, S. *et al.* Clonal culturing of human embryonic stem cells on laminin-521/E-cadherin matrix in defined and xeno-free environment. *Nat. Commun.* **5,** 3195 (2014).
14. Prowse, A. B. *et al.* Long term culture of human embryonic stem cells on recombinant vitronectin in ascorbate free media. *Biomaterials* **31,** 8281–8288 (2010).
15. Yap, L. Y. *et al.* Defining a threshold surface density of vitronectin for the stable expansion of human embryonic stem cells. *Tissue Eng. Part C* **17,** 193–207 (2011).
16. Heng, B. C. *et al.* Translating human embryonic stem cells from 2-dimensional to 3-dimensional cultures in a defined medium on laminin- and vitronectin-coated surfaces. *Stem Cells Develop.* **21,** 1701–1715 (2012).
17. Lu, H. F. *et al.* A defined xeno-free and feeder-free culture system for the derivation, expansion and direct differentiation of transgene-free patient-specific induced pluripotent stem cells. *Biomaterials* **35,** 2816–2826 (2014).
18. Manton, K. J. *et al.* A chimeric vitronectin: IGF-I protein supports feeder-cell-free and serum-free culture of human embryonic stem cells. *Stem Cells Develop.* **19,** 1297–1305 (2010).
19. Liu, L. *et al.* Nanofibrous gelatin substrates for long-term expansion of human pluripotent stem cells. *Biomaterials* **35,** 6259–6267 (2014).
20. Braam, S. R. *et al.* Recombinant vitronectin is a functionally defined substrate that supports human embryonic stem cell self-renewal via alphavbeta5 integrin. *Stem Cells* **26,** 2257–2265 (2008).
21. Jonas, S. J. *et al.* A spatially and chemically defined platform for the uniform growth of human pluripotent stem cells. *Mat. Sci. Eng. C* **33,** 234–241 (2013).
22. Meng, G., Liu, S. & Rancourt, D. E. Synergistic effect of medium, matrix, and exogenous factors on the adhesion and growth of human pluripotent stem cells under defined, xeno-free conditions. *Stem Cells Dev.* **21,** 2036–2048 (2012).
23. Hayashi, Y. *et al.* Reduction of N-glycolylneuraminic acid in human induced pluripotent stem cells generated or cultured under feeder- and serum-free defined conditions. *PLoS One* **5,** e14099 (2010).
24. Swistowski, A. *et al.* Xeno-free defined conditions for culture of human embryonic stem cells, neural stem cells and dopaminergic neurons derived from them. *PLoS One* **4,** e6233 (2009).
25. Melkoumian, Z. *et al.* Synthetic peptide-acrylate surfaces for long-term self-renewal and cardiomyocyte differentiation of human embryonic stem cells. *Nat. Biotech.* **28,** 606–610 (2010).

26. Higuchi, A. *et al.* Preparation of induced pluripotent stem cells on dishes grafted on oligopeptide under feeder-free conditions. *J. Taiwan Inst. Chem. Eng.* **45,** 295–301 (2014).
27. Kolhar, P., Kotamraju, V. R., Hikita, S. T., Clegg, D. O. & Ruoslahti, E. Synthetic surfaces for human embryonic stem cell culture. *J. Biotechnol.* **146,** 143–146 (2010).
28. Nishishita, N. *et al.* Generation of virus-free induced pluripotent stem cell clones on a synthetic matrix via a single cell subcloning in the naive state. *PLoS One* **7,** e38389 (2012).
29. Jin, S., Yao, H., Weber, J. L., Melkoumian, Z. K. & Ye, K. A synthetic, xeno-free peptide surface for expansion and directed differentiation of human induced pluripotent stem cells. *PLoS One* **7,** e50880 (2012).
30. Lin, P. Y. *et al.* A synthetic peptide-acrylate surface for production of insulin-producing cells from human embryonic stem cells. *Stem Cells Dev.* **23,** 372–379 (2014).
31. Pennington, B. O., Clegg, D. O., Melkoumian, Z. K. & Hikita, S. T. Defined culture of human embryonic stem cells and xeno-free derivation of retinal pigmented epithelial cells on a novel, synthetic substrate. *Stem Cells Transl. Med.* **4,** 165–177 (2015).
32. Klim, J. R., Li, L., Wrighton, P. J., Piekarczyk, M. S. & Kiessling, L. L. A defined glycosaminoglycan-binding substratum for human pluripotent stem cells. *Nat. Methods* **7,** 989–994 (2010).
33. Musah, S. *et al.* Glycosaminoglycan-binding hydrogels enable mechanical control of human pluripotent stem cell self-renewal. *ACS Nano* **6,** 10168–10177 (2012).
34. Deng, Y. *et al.* Long-term self-renewal of human pluripotent stem cells on peptide-decorated poly(OEGMA-co-HEMA) brushes under fully defined conditions. *Acta Biomater.* **9,** 8840–8850 (2013).
35. Fan, Y., Hsiung, M., Cheng, C. & Tzanakakis, E. S. Facile engineering of xeno-free microcarriers for the scalable cultivation of human pluripotent stem cells in stirred suspension. *Tissue Eng. Part A* **20,** 588–599 (2014).
36. Wu, S. *et al.* Spider silk for xeno-free long-term self-renewal and differentiation of human pluripotent stem cells. *Biomaterials* **35,** 8496–8502 (2014).
37. Chen, X. *et al.* Thermoresponsive worms for expansion and release of human embryonic stem cells. *Biomacromolecules* **15,** 844–855 (2014).
38. Park, H. J. *et al.* Bio-inspired oligovitronectin-grafted surface for enhanced self-renewal and long-term maintenance of human pluripotent stem cells under feeder-free conditions. *Biomaterials* **50,** 127–139 (2015).
39. Brafman, D. A. *et al.* Long-term human pluripotent stem cell self-renewal on synthetic polymer surfaces. *Biomaterials* **31,** 9135–9144 (2010).
40. Nandivada, H. *et al.* Fabrication of synthetic polymer coatings and their use in feeder-free culture of human embryonic stem cells. *Nat. Protoc.* **6,** 1037–1043 (2011).
41. Ross, A. M., Nandivada, H., Ryan, A. L. & Lahann, J. Synthetic substrates for long-term stem cell culture. *Polymer* **53,** 2533–2639 (2012).
42. Qian, X., Villa-Diaz, L. G., Kumar, R., Lahann, J. & Krebsbach, P. H. Enhancement of the propagation of human embryonic stem cells by modifications in the gel architecture of PMEDSAH polymer coatings. *Biomaterials* **35,** 9581–9590 (2014).
43. Villa-Diaz, L. G. *et al.* Synthetic polymer coatings for long-term growth of human embryonic stem cells. *Nat. Biotech.* **28,** 581–583 (2010).
44. Irwin, E. F., Gupta, R., Dashti, D. C. & Healy, K. E. Engineered polymer-media interfaces for the long-term self-renewal of human embryonic stem cells. *Biomaterials* **32,** 6912–6919 (2011).
45. Zhang, R. *et al.* A thermoresponsive and chemically defined hydrogel for long-term culture of human embryonic stem cells. *Nat. Commun.* **4,** 1335 (2013).
46. Engler, A. J., Sen, S., Sweeney, H. L. & Discher, D. E. Matrix elasticity directs stem cell lineage specification. *Cell* **126,** 677–689 (2006).
47. Higuchi, A., Ling, Q. D., Chang, Y., Hsu, S. T. & Umezawa, A. Physical cues of biomaterials guide stem cell differentiation fate. *Chem. Rev.* **113,** 3297–3328 (2013).
48. Kumar, S. S. *et al.* The combined influence of substrate elasticity and surface-grafted molecules on the *ex vivo* expansion of hematopoietic stem and progenitor cells. *Biomaterials* **34,** 7632–7644 (2013).
49. Huebsch, N. *et al.* Harnessing traction-mediated manipulation of the cell/matrix interface to control stem-cell fate. *Nat. Mater.* **9,** 518–626 (2010).
50. Trappmann, B. *et al.* Extracellular-matrix tethering regulates stem-cell fate. *Nat. Mater.* **10,** 979–987 (2012).
51. Chowdhury, F. *et al.* Soft substrates promote homogeneous self-renewal of embryonic stem cells via downregulating cell-matrix tractions. *PLoS One* **5,** e15655 (2010).
52. Dementjev, A. P. *et al.* X-ray photoelectron spectroscopy reference data for identification of the C3N4 phase in carbon-nitrogen films. *Diam. Relat. Mater.* **9,** 1904–1907 (2000).
53. Nagaoka, M., Si-Tayeb, K., Akaike, T. & Duncan, S. A. Culture of human pluripotent stem cells using completely defined conditions on a recombinant E-cadherin substratum. *BMC Develop. Biol.* **10,** 60 (2010).
54. Stephenson, E. *et al.* Derivation and propagation of human embryonic stem cell lines from frozen embryos in an animal product-free environment. *Nat. Protoc.* **7,** 1366–1381 (2012).
55. Chang, C. W. *et al.* Engineering cell-material interfaces for long-term expansion of human pluripotent stem cells. *Biomaterials* **34,** 912–921 (2013).
56. Suemori, H. *et al.* Efficient establishment of human embryonic stem cell lines and long-term maintenance with stable karyotype by enzymatic bulk passage. *Biochem. Biophys. Res. Commun.* **345,** 926–932 (2006).

Acknowledgements

This research was partially supported by the Ministry of Science and Technology under Grant numbers 103-2120-M-008-001 and 104-2221-E-008-107-MY3. This work was also supported by the LandSeed Hospital project (103LSH-NCU-1 and NCU-LSH-104-A-001) and the Cathay General Hospital Project (CGH-MR-A10404, CGH-MR-A10405, and 104CGH-NCU-A3). We acknowledge the International High Cited Research Group (IHCRG #14-104), Deanship of Scientific Research, King Saud University, Riyadh, Kingdom of Saudi Arabia. A Grant-in-Aid for Scientific Research (15K06591) from the Ministry of Education, Culture, Sports, Science, and Technology of Japan is also acknowledged.

Author Contributions

A.H. participated in the design and interpretation of the study, drafting and revising the manuscript, and provided administrative, technical, and supervisory support. Q.D.L. and S.S.K. collected and summarized the results. S.H.K., H.F.L. and Y.M.C. prepared the hydrogels and cultured the hPSCs. A.A.A., M.A.M. and S.C.C. performed the experiments investigating the differentiation and characterization of hPSCs. K.M., H.C.L. and S.T.H. participated in the interpretation of the results and constructed the Figures. A.U. edited the manuscript.

Additional Information

Supplementary information accompanies this paper at http://www.nature.com/srep

Competing financial interests: The authors declare no competing financial interests.

How to cite this article: Higuchi, A. *et al.* Long-term xeno-free culture of human pluripotent stem cells on hydrogels with optimal elasticity. *Sci. Rep.* **5**, 18136; doi: 10.1038/srep18136 (2015).

D1000–D1004 *Nucleic Acids Research, 2016, Vol. 44, Database issue* *Published online 22 October 2015*
doi: 10.1093/nar/gkv1096

OpenTein: a database of digital whole-slide images of stem cell-derived teratomas

Sung-Joon Park[1], Yusuke Komiyama[1], Hirofumi Suemori[2], Akihiro Umezawa[3] and Kenta Nakai[1,*]

[1]Human Genome Center, The Institute of Medical Science, The University of Tokyo, 4-6-1 Shirokanedai, Minato-ku, Tokyo 108-8639, Japan, [2]Department of Embryonic Stem Cell Research, Institute for Frontier Medical Sciences, Kyoto University, 53 Kawahara-cho, Shogoin, Sakyo-ku, Kyoto 606-8507, Japan and [3]Department of Reproductive Biology, National Institute for Child Health and Development, 2-10-1 Okura, Setagaya-ku, Tokyo 157-8535, Japan

Received August 14, 2015; Revised October 07, 2015; Accepted October 11, 2015

ABSTRACT

Human stem cells are promising sources for regenerative therapy. To ensure safety of future therapeutic applications, the differentiation potency of stem cells has to be tested and be widely opened to the public. The potency is generally assessed by teratoma formation comprising differentiated cells from all three germ layers, and the teratomas can be inspected through high-quality digital images. The teratoma assay, however, lacks consistency in transplantation protocols and even in interpretation, which needs community-based efforts for improving the assay quality. Here, we have developed a novel database OpenTein (Open Teratoma Investigation, http://opentein.hgc.jp/) to archive and freely distribute high-resolution whole-slide images and relevant records. OpenTein has been designed as a searchable, zoomable and annotatable web-based repository system. We have deposited 468 images of teratomas derived by our transplantation of human stem cells, and users can freely access and process such digital teratoma images. Approximately, the current version of OpenTein responds within 11.2 min for processing 2.03 gigapixel teratoma images. Our system offers valuable tools and resources in the new era of stem cell biology.

INTRODUCTION

Human embryonic stem cells (hESCs) and human induced-pluripotent stem cells (hiPSCs) are promising sources for stem cell biology and regenerative therapy. Prior to the practical use of the stem cells, it is important to characterize their pluripotency *in vivo* for safety and success in further applications (1,2). In general, the transplantation of human stem cells into immuno-deficient animals is used to demonstrate the capacity of cell pluripotency, which forms teratomas comprising differentiated cells from all three germ layers (3–5). Recently, high-quality microscopes providing digital whole-slide images (WSIs) facilitate the inspection of teratoma histologic features (6), and WSIs are becoming a highly valuable resource because they also offer insights into the mechanisms of tissue development (7).

Unfortunately, while the teratoma assay is considered as the '*gold standard*' for pluripotency tests, this assay lacks consistency in experimental protocols, leading to contradictory assessments and poor reproducibility (1,8). This is due in part to the variability of experimental parameters (e.g. the number of cells injected, injection sites and growth conditions) that potentially affect the results of histopathological analysis. In addition, journal publications that detail only a representative image of teratomas cannot bring out the potential of teratoma formation assay; it is unclear whether derivatives of all germ layers are found in the same section of teratomas. Although efforts have been made to standardize the teratoma assay (2,8,9), no community-based attempts have been made to archive and freely distribute the protocols, resultant WSIs and expert histological assessments. As learnt from public repositories, such attempts enhance not only the fundamentals of qualitative and quantitative assays but also transparent reproducibility and accessibility (10–12).

Here, we have developed a database OpenTein (Open Teratoma Investigation) having web-based features as a public repository system. Like other repositories (13), OpenTein requires user registration for manipulating the teratoma assays including WSIs and relevant records. Along with assigning unique identifiers, OpenTein automatically creates web pages containing zoomable and annotatable high-resolution digital images in a vendor-independent fashion. Thereby, users can easily share and promote their teratoma assays through the internet. We have currently deposited 468 assays derived by our transplantation (4,5), consisting

*To whom correspondence should be addressed. Tel: +81 3 5449 5131; Fax: +81 3 5449 5133; Email: knakai@ims.u-tokyo.ac.jp

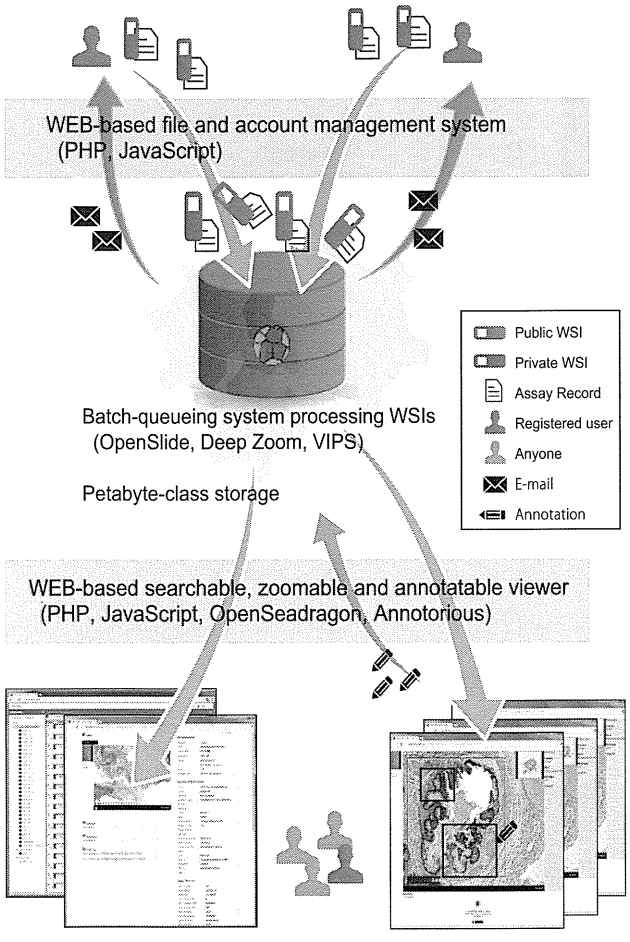

Figure 1. A schematic representation of OpenTein as a repository system of the teratoma assay.

of 52 for hESCs and 416 for hiPSCs. Anyone can freely access the valuable resource at http://opentein.hgc.jp.

SYSTEM OVERVIEW

Interactive web-based platform

OpenTein has been designed to make WSIs accessible to users who lack computational resources; the file size of WSIs is massive ranging from several hundred megabytes to several gigabytes (14), which impacts the storage capacity of cost-intensive commercial server systems. In parallel, OpenTein has been intended to offer users traceable and annotatable teratoma assays. As shown in several studies (14,15), the WSIs can be systematically managed by using open-source libraries. Thus, such well-organized resources can be used for various purposes; e.g. quantitative assays and the automatic identification of histological features (16,17).

As illustrated in Figure 1, OpenTein that has been installed on a supercomputer with petabyte-class storage provides the interactive web-based interface for freely registering accounts and easily depositing the assays. Registered users can specify the sharing mode of uploaded assays; i.e. public or private (hidden from other users). For individual public assays, OpenTein assigns a unique accession number beginning with 'OTi', which provides accessibility if the accession numbers are cited in journal publications, for example. In addition, to help users share comments and annotations, OpenTein embedded the Facebook comment plugin and equipped an online annotation tool. When the processing of uploaded WSIs was finished and annotations were modified by other users, OpenTein sends e-mail messages to owners.

Table 1. List of features available for each user type

	Registered user		Non-registered user
	Public	Private	Public
Search	Yes	Yes	Yes
Browse	Yes	Yes	Yes
Annotation	Yes	Yes	Yes*
File download	Yes	Yes	Yes
File upload	Yes	Yes	
E-mail notice	Yes	Yes	
Delivery	Yes	Yes	
Accession Number	Yes		

*not saved in the OpenTein database.

Key features

OpenTein was built by the programming language PHP and JavaScript. The system automatically processes WSIs by submitting batch jobs to create multilayered pyramid images with smaller tile images, which is the most time-consuming step and allows users to pan and zoom at various magnifications by manipulating the mouse of a computer. This processing utilizes vendor-neutral image software, i.e. OpenSlide (18) running by VIPS (ver. 7.42, http://libvips.blogspot.jp/). We currently accept the following file formats; Aperio SVS, Hamamatsu NDPI, Leica SCN and generic TIFF. The web-based WSI viewer has been implemented with open-source JavaScript OpenSeadragon (https://openseadragon.github.io/) and Annotorious (http://annotorious.github.io/) coupled with in-house developed APIs.

As summarized in Table 1, anyone can explore and access public assays through search and annotation options, although annotations by non-registered users are not stored in OpenTein to prevent vandals. Therefore, the user registration with a valid e-mail address is important to effectively use our system. In addition, we prepared a delivery function that a registered user can send WSIs to another registered user. This feature helps seamless collaboration of users. For instance, researchers who have imaging facilities digitalize teratomas and pass WSIs to sample providers who do not have such facilities.

It is important to note that for ethics' sake OpenTein monitors any events occurring on all deposited assays even on private assays.

WEB INTERFACE

Since a teratoma assay often involves a series of WSIs, we manage users' depositions as a hierarchical data tree that has clickable multilevel nodes; e.g. in the public interface 'Browser' (Figure 2A), 'All' (root node), 'Owner' (registered user ID), 'Project' (a group of assays) and assay (end node). For each of the registered users, we prepared a special

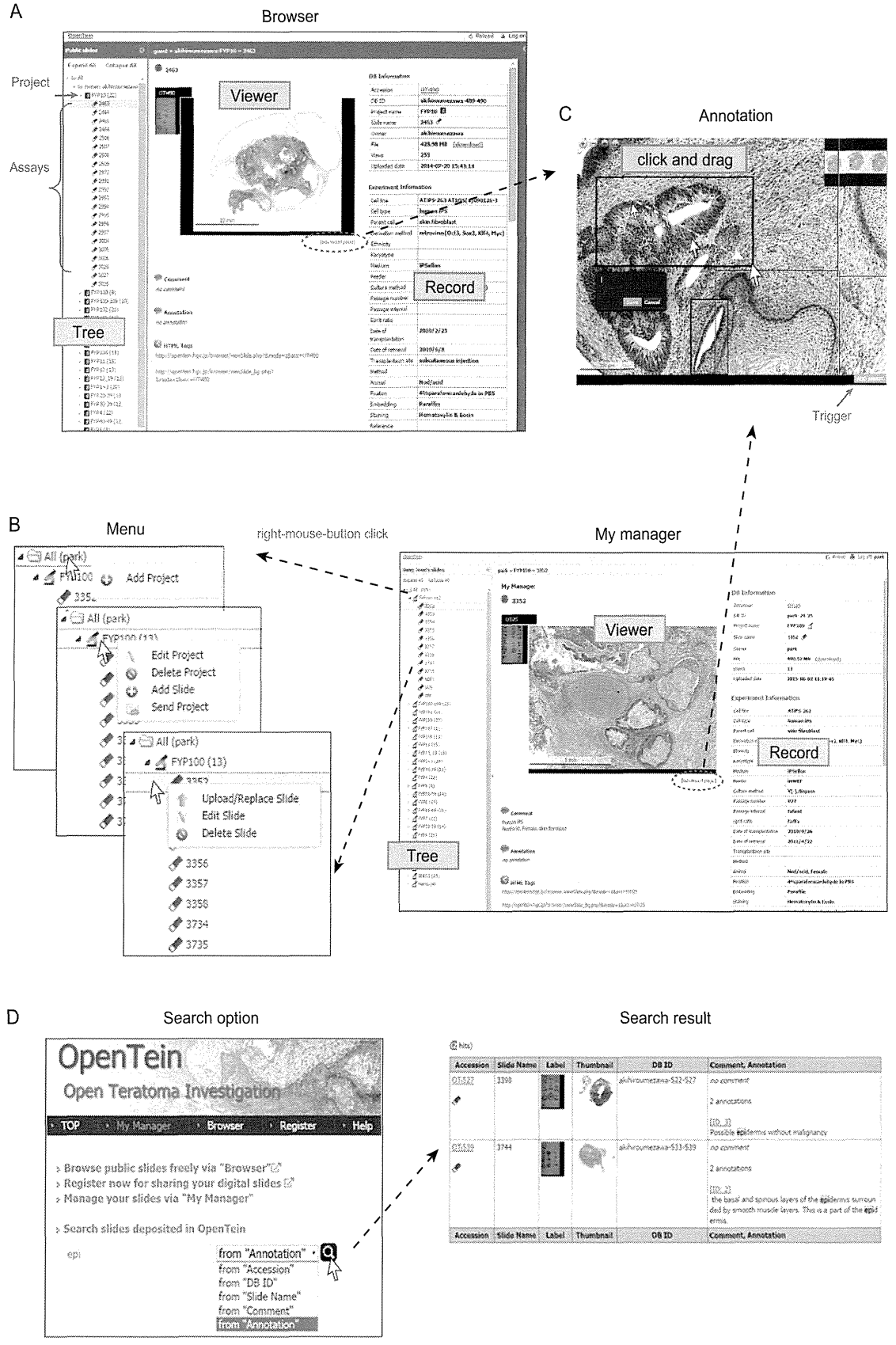

Figure 2. Screenshots of the web-based interface. (**A**) Anyone can explore the public assays through 'Browser' implemented with a hierarchical data tree. (**B**) Registered users can work through the interface 'My manager'. (**C**) The annotation can be simply done by drawing a rectangle for a region of interest. (**D**) The search option enables easy access to deposited assays.

workspace, namely 'My manager'. In this workspace, users can control assays by clicking the right-mouse-button on the tree nodes after login to OpenTein (Figure 2B). Clicking the menu items 'Add Slide' and 'Edit Slide' (Figure 2B) shows pop-up windows that enable users to enter and modify the corresponding experimental details. The required experimental details have been chosen based on our empirical knowledge, which needs further community-based discussions for standardizing the minimum information (11,12) that must be reported for the interpretability and reproducibility.

For annotating WSIs, whenever the trigger button 'Add annot.' is available on the viewer, one can mark a region of interest by drawing a rectangle and then can comment it (Figure 2C). If an annotation was created by a registered user, OpenTein assigns a unique ID for it. Although the annotations are hyperlinked from Browser and My manager, they can be specified by the internet URLs. Alternative is the search option that allows users to query such as annotation from registered users, accession number, database ID, slide name described by owners and comment provided by owners (Figure 2D). Registered users can find private assays also by the search option after login.

Users can find more instructions from the FAQ (Frequently Asked Questions) website at http://opentein.hgc.jp/FAQ/faq.php.

PROCESSING OF WHOLE-SLIDE IMAGE

Impact of a tile size on storage

To help users quickly zoom in on different parts of the high-resolution image, OpenTein runs VIPS to process WSIs into small JPEG tiles in Deep Zoom format, and the tile size (e.g. 256 × 256 pixels) is an important factor for the performance of our system. By using the 468 WSIs in SVS file format we deposited to OpenTein, we confirmed that the total number of tiles created from single SVS file is depending on the original resolution and the tile size (Supplementary Figure S1A). The total file size of tiles became approximately 1.5 times larger than that of the original SVS file (Supplementary Figure S1B); on average, 590.7 megabyte (MB) SVS file is converted into 982.4, 900.4 and 873.6 MB tiles in 256, 512 and 1024 tile size, respectively. These results suggest that tiling WSIs into 256 × 256 pixel images requires huge file quotas, and that the requirement of storage capacity is not dramatically changed among different tile sizes. A bigger tile size (e.g. 1024 × 1024 pixels) will lead to dissatisfaction, since users need a longer time to load such heavy tiles. We set it to 512 in here.

Response times

The processing of uploaded WSIs is executed on a system that has been built with 2 terabyte (TB) memory and 48 cores of 3.0 GHz Intel CPU E7-8857. As shown in Supplementary Figure S1C, WSI resolutions affect the response time that is the elapsed time from start to end of a submitted batch job. Although such response times can be reduced by dividing a process into several multiple tasks simultaneously running (i.e. threads), larger number of threads requires more memory that is almost constant against the WSI resolutions (Supplementary Figure S1D). We set the number of threads to 12 in here.

On average, the current version of OpenTein running with 12 threads that require 8.02 gigabyte (GB) memory responds within 11.2 min when one finished uploading a 2.03 gigapixel WSI (590.7 MB), and generates 9936.1 tiles in 512 × 512 pixels (900.4 MB in total file size).

CONCLUSIONS

Although alternatives exist (e.g. gene expression profiling and the tetraploid complementation assay), the teratoma assay is widely used for proving pluripotency of human stem cells. To archive the teratoma assays and to share them enhance the fundamentals of effective pluripotency tests. For accomplishing this, we developed a database OpenTein that makes high-resolution WSIs and relevant notes uploadable, accessible and traceable to public users. In this study, we have deposited 468 WSIs delivered by our experiments, and anyone can use this resource through the user-friendly web interface.

For its further progress, community-based efforts are indispensable as expert histological assessments need the time and interpretative efforts. In this regard, to implement computational algorithms that aid the expert investigation to succeed is challenging but worthwhile. To improve its usability, we aim to further design web-based interfaces for several features, such as uploading multiple files at a time and annotating by various shapes and colors. Moreover, transferring data in human- and machine-readable formats is important to systematically manage the assays, which helps to guide the minimum information that ensures the interpretability and reproducibility. We believe that such well-structured records along with data sharing will enhance stem cell biology and regenerative therapy.

SUPPLEMENTARY DATA

Supplementary Data are available at NAR Online.

ACKNOWLEDGEMENTS

The authors thank Emi Ikeda (The Institute of Medical Science, The University of Tokyo) and Kayoko Saito (National Institute for Child Health and Development) for helping the system installation. The database was developed on the supercomputer system at Human Genome Center, The Institute of Medical Science, The University of Tokyo.

FUNDING

Research on Regenerative Medicine for Clinical Application, Health and Labour Sciences Research Grants, Japan and Grant-in-Aid for Scientific Research [(B) 15H04715]. Funding for open access charge: Grant-in-Aid for Scientific Research [(B) 15H04715, Japan].
Conflict of interest statement. None declared.

REFERENCES

1. Buta,C., David,R., Dressel,R., Emgard,M., Fuchs,C., Gross,U., Healy,L., Hescheler,J., Kolar,R., Martin,U. *et al.* (2013)

Reconsidering pluripotency tests: do we still need teratoma assays? *Stem Cell Res.*, **11**, 552–562.
2. Prokhorova,T.A., Harkness,L.M., Frandsen,U., Ditzel,N., Schroder,H.D., Burns,J.S. and Kassem,M. (2009) Teratoma formation by human embryonic stem cells is site dependent and enhanced by the presence of Matrigel. *Stem Cells Dev.*, **18**, 47–54.
3. Thomson,J.A., Itskovitz-Eldor,J., Shapiro,S.S., Waknitz,M.A., Swiergiel,J.J., Marshall,V.S. and Jones,J.M. (1998) Embryonic stem cell lines derived from human blastocysts. *Science*, **282**, 1145–1147.
4. Suemori,H., Tada,T., Torii,R., Hosoi,Y., Kobayashi,K., Imahie,H., Kondo,Y., Iritani,A. and Nakatsuji,N. (2001) Establishment of embryonic stem cell lines from cynomolgus monkey blastocysts produced by IVF or ICSI. *Dev. Dyn.*, **222**, 273–279.
5. Akutsu,H., Machida,M., Kanzaki,S., Sugawara,T., Ohkura,T., Nakamura,N., Yamazaki-Inoue,M., Miura,T., Vemuri,M.C., Rao,M.S. *et al.* (2015) Xenogeneic-free defined conditions for derivation and expansion of human embryonic stem cells with mesenchymal stem cells. *Regenerative Ther.*, **1**, 18–29.
6. Farahani,N., Parwani,A.V. and Pantanowitz,L. (2015) Whole slide imaging in pathology: advantages, limitations, and emerging perspectives. *Pathol. Lab Med. Int.*, **7**, 23–33.
7. Muller,F.J., Goldmann,J., Loser,P. and Loring,J.F. (2010) A call to standardize teratoma assays used to define human pluripotent cell lines. *Cell Stem Cell*, **6**, 412–414.
8. Gropp,M., Shilo,V., Vainer,G., Gov,M., Gil,Y., Khaner,H., Matzrafi,L., Idelson,M., Kopolovic,J., Zak,N.B. *et al.* (2012) Standardization of the teratoma assay for analysis of pluripotency of human ES cells and biosafety of their differentiated progeny. *PLoS One*, **7**, e45532.
9. Nelakanti,R.V., Kooreman,N.G. and Wu,J.C. (2015) Teratoma formation: a tool for monitoring pluripotency in stem cell research. *Curr. Protoc. Stem Cell Biol.*, **32**, 4A.8.1–4A.8.17.
10. Brazma,A., Hingamp,P., Quackenbush,J., Sherlock,G., Spellman,P., Stoeckert,C., Aach,J., Ansorge,W., Ball,C.A., Causton,H.C. *et al.* (2001) Minimum information about a microarray experiment (MIAME)-toward standards for microarray data. *Nat. Genet.*, **29**, 365–371.
11. Deutsch,E.W., Ball,C.A., Berman,J.J., Bova,G.S., Brazma,A., Bumgarner,R.E., Campbell,D., Causton,H.C., Christiansen,J.H., Daian,F. *et al.* (2008) Minimum information specification for in situ hybridization and immunohistochemistry experiments (MISFISHIE). *Nat. Biotechnol.*, **26**, 305–312.
12. Nekrutenko,A. and Taylor,J. (2012) Next-generation sequencing data interpretation: enhancing reproducibility and accessibility. *Nat. Rev. Genet.*, **13**, 667–672.
13. Kodama,Y., Mashima,J., Kosuge,T., Katayama,T., Fujisawa,T., Kaminuma,E., Ogasawara,O., Okubo,K., Takagi,T. and Nakamura,Y. (2015) The DDBJ Japanese genotype-phenotype archive for genetic and phenotypic human data. *Nucleic Acids Res.*, **43**, D18–D22.
14. Gutman,D.A., Cobb,J., Somanna,D., Park,Y., Wang,F., Kurc,T., Saltz,J.H., Brat,D.J. and Cooper,L.A. (2013) Cancer digital slide archive: an informatics resource to support integrated in silico analysis of TCGA pathology data. *J. Am. Med. Inform. Assoc.*, **20**, 1091–1098.
15. Igarashi,Y., Nakatsu,N., Yamashita,T., Ono,A., Ohno,Y., Urushidani,T. and Yamada,H. (2015) Open TG-GATEs: a large-scale toxicogenomics database. *Nucleic Acids Res.*, **43**, D921–D927.
16. Avior,Y., Biancotti,J.C. and Benvenisty,N. (2015) TeratoScore: assessing the differentiation potential of human pluripotent stem cells by quantitative expression analysis of teratomas. *Stem Cell Rep.*, **4**, 967–974.
17. Bhagavatula,R., Fickus,M., Kelly,W., Guo,C., Ozolek,J.A., Castro,C.A. and Kovacevic,J. (2010) Automatic identification and delineation of germ layer components in H&E stained images of teratomas derived from human and nonhuman primate embryonic stem cells. *Proc. IEEE Int. Symp. Biomed. Imaging*, **2010**, 1041–1044.
18. Goode,A., Gilbert,B., Harkes,J., Jukic,D. and Satyanarayanan,M. (2013) OpenSlide: a vendor-neutral software foundation for digital pathology. *J. Pathol. Inform.*, **4**, 27.

© 2015. Published by The Company of Biologists Ltd | Biology Open (2015) 4, 1595-1607 doi:10.1242/bio.013151

METHODS & TECHNIQUES

Generation of primitive neural stem cells from human fibroblasts using a defined set of factors

Takumi Miura[1,*,‡], Tohru Sugawara[1], Atsushi Fukuda[1], Ryo Tamoto[1], Tomoyuki Kawasaki[1], Akihiro Umezawa[1] and Hidenori Akutsu[1,2,‡]

ABSTRACT

In mice, leukemia inhibitory factor (LIF)-dependent primitive neural stem cells (NSCs) have a higher neurogenic potential than bFGF-dependent definitive NSCs. Therefore, expandable primitive NSCs are required for research and for the development of therapeutic strategies for neurological diseases. There is a dearth of suitable techniques for the generation of human long-term expandable primitive NSCs. Here, we have described a method for the conversion of human fibroblasts to LIF-dependent primitive NSCs using a strategy based on techniques for the generation of induced pluripotent stem cells (iPSCs). These LIF-dependent induced NSCs (LD-iNSCs) can be expanded for >100 passages. Long-term cultured LD-iNSCs demonstrated multipotent neural differentiation potential and could generate motor neurons and dopaminergic neurons, as well as astrocytes and oligodendrocytes, indicating a high level of plasticity. Furthermore, LD-iNSCs easily reverted to human iPSCs, indicating that LD-iNSCs are in an intermediate iPSC state. This method may facilitate the generation of patient-specific human neurons for studies and treatment of neurodegenerative diseases.

KEY WORDS: Neural stem cell, Reprogramming, Stem cells

INTRODUCTION

Yamanaka's discovery of induced pluripotent stem cells (iPSCs) was a breakthrough innovation in the field of cellular reprogramming, which is the conversion of differentiated cells into an undifferentiated state (Takahashi et al., 2007; Takahashi and Yamanaka, 2006). Concepts emerging from iPSC technology have provided valuable opportunities for the expansion of research on transdifferentiation, or the irreversible conversion of a specific cell type to another via forced expression of lineage-related transcription factors (Caiazzo et al., 2011; Efe et al., 2011; Huang et al., 2011; Ieda et al., 2010; Pang et al., 2011; Pereira et al., 2013; Pfisterer et al., 2011; Vierbuchen et al., 2010; Yoo et al., 2011). Therefore, cells converted into a desired cell type could be useful as a new tool for the discovery of therapeutic targets and pathogenic processes. Nonetheless, because most of the converted cells are terminally differentiated, their proliferation potential is much lower compared to that of multipotent stem cells, suggesting that direct lineage conversion technology has limitations in drug screening or autologous cell therapy. To address this issue, direct conversion of somatic cells to lineage-committed multipotent stem cells might be an attractive approach for indirect generation of desired cell types. This indirect approach would allow for the production of sufficient amounts of cells for basic research, drug screening, disease modeling, or cell therapy.

Some researchers have recently reported that multipotent neural stem/progenitor cells (NSCs) can be directly induced from fibroblasts using neural progenitor-specific transcription factors or the Yamanaka factors as reprogramming agents (Han et al., 2012; Kim et al., 2011; Lujan et al., 2012; Ring et al., 2012; Thier et al., 2012; Wang et al., 2013). These induced neural stem/progenitor cells (iNSCs) are cultured in a standard neural stem cell medium supplemented with basic fibroblast growth factor (bFGF) and epidermal growth factor (EGF). Under these culture conditions, the transition of NSCs into a glia-restricted precursor state occurs over time (Qian et al., 2000). These observations suggest that the neurogenic potential of bFGF-dependent definitive NSCs may be diminished by environmental factors. On the other hand, the earliest mammalian NSCs (primitive NSCs) can differentiate from pluripotent embryonic stem cells (ESCs). Primitive NSCs have more diverse developmental opportunities in neural lineages than definitive NSCs. These primitive NSCs emerge in response to leukemia inhibitory factor (LIF), have distinct growth factor requirements, express neural precursor markers, generate neurons and glia *in vitro*, and have a neural and non-neural lineage potential *in vivo* (Li et al., 2011; Tropepe et al., 2001). Recently, a combination of Yamanaka factors and small molecules was shown to directly convert human fibroblasts into LIF-dependent neural progenitors (NPs), using a nonintegrating method (Lu et al., 2013). Nonetheless, these LIF-dependent induced NPs (iNPs) gradually lose their ability to be re-specified to other fates during long-term passaging (>20 passages). This phenomenon indicates that persistent expression of exogenous reprogramming factors may be required for the maintenance of neurogenic potential in iNPs.

In this study, we present a novel method for the generation of self-renewable, multipotent, and neural lineage-restricted LIF-dependent induced primitive NSCs (LD-iNSCs) from human fibroblasts. These LD-iNSCs exhibit a characteristic morphology, gene expression patterns, and growth rate, as well as a predictable *in vitro* differentiation potential. Specifically, these stable, expandable LD-iNSC clones possess the plasticity of NSCs and can differentiate into neurons (motor neurons and dopaminergic neurons), astrocytes, and oligodendrocytes. Furthermore, LD-iNSCs retain high neurogenic potential even after long-term expansion and repeated passaging in the presence of LIF, CHIR99021 and PD0325901. Our results demonstrate that expandable human primitive NSCs can be directly generated from

[1]Department of Reproductive Biology, National Center for Child Health and Development, Tokyo 157-8535, Japan. [2]Department of Stem Cell Research, Fukushima Medical University, Fukushima 960-1295, Japan.
*Present address: Division of Cell-Based Therapeutic Products, National Institute of Health Sciences, Tokyo 158-8501, Japan.

‡Authors for correspondence (miura-t@nihs.go.jp; akutsu-h@ncchd.go.jp)

Received 25 June 2015; Accepted 21 September 2015

Biology Open (2015) 4, 1595-1607 doi:10.1242/bio.013151

somatic cells using the same factors known to reprogram cells for pluripotency, under special conditions.

RESULTS

LD-iNSCs are directly induced from human fibroblasts by five factors with two inhibitors (2i)

A recent report indicated that LIF-dependent human primitive neural stem cells differentiate from hiPSCs in a chemically defined medium containing LIF and two inhibitors (MEK1/MEK2 inhibitor PD0325901 and GSK-3β inhibitor CHIR99021), collectively termed 2i (Hirano et al., 2012). In this study, we generated LIF-dependent human iNSCs from adult tissues using the doxycycline (Dox)-inducible lentiviral vector transduction method: human fibroblasts were infected with lentivirus-containing reprogramming factors. Our protocol for the generation of human iNSCs in the presence of LIF is shown in Fig. 1A and B. We first analyzed the ability of the reprogramming factors to directly reprogram human fibroblasts to NSCs. To efficiently introduce reprogramming factors into human fibroblasts (endometrial fibrotic stromal cells), we generated polycistronic viral vectors that would express either four (*OCT4*, *KLF4*, *SOX2* and *L-MYC*) or five (*OCT4*, *KLF4*, *SOX2*, *L-MYC* and *NANOG*) reprogramming genes from a single promoter using 2A peptides and internal ribosomal entry sites (IRES). The generation efficiency of iNSCs was assessed using an assay for alkaline phosphatase-positive colonies, based on a previous report that LIF-dependent primitive NSCs derived from hESCs are positive for alkaline phosphatase (Li et al., 2011). As shown in Fig. S1, endogenous alkaline phosphatase-positive colonies effectively emerged after treatment with the five reprogramming factors, but not with only four factors. Reprogramming of human fibroblasts in the presence of LIF using this lentiviral vector (five reprogramming factors) resulted in the formation of round colonies, starting approximately two weeks after the addition of Dox. Subsequently, these round

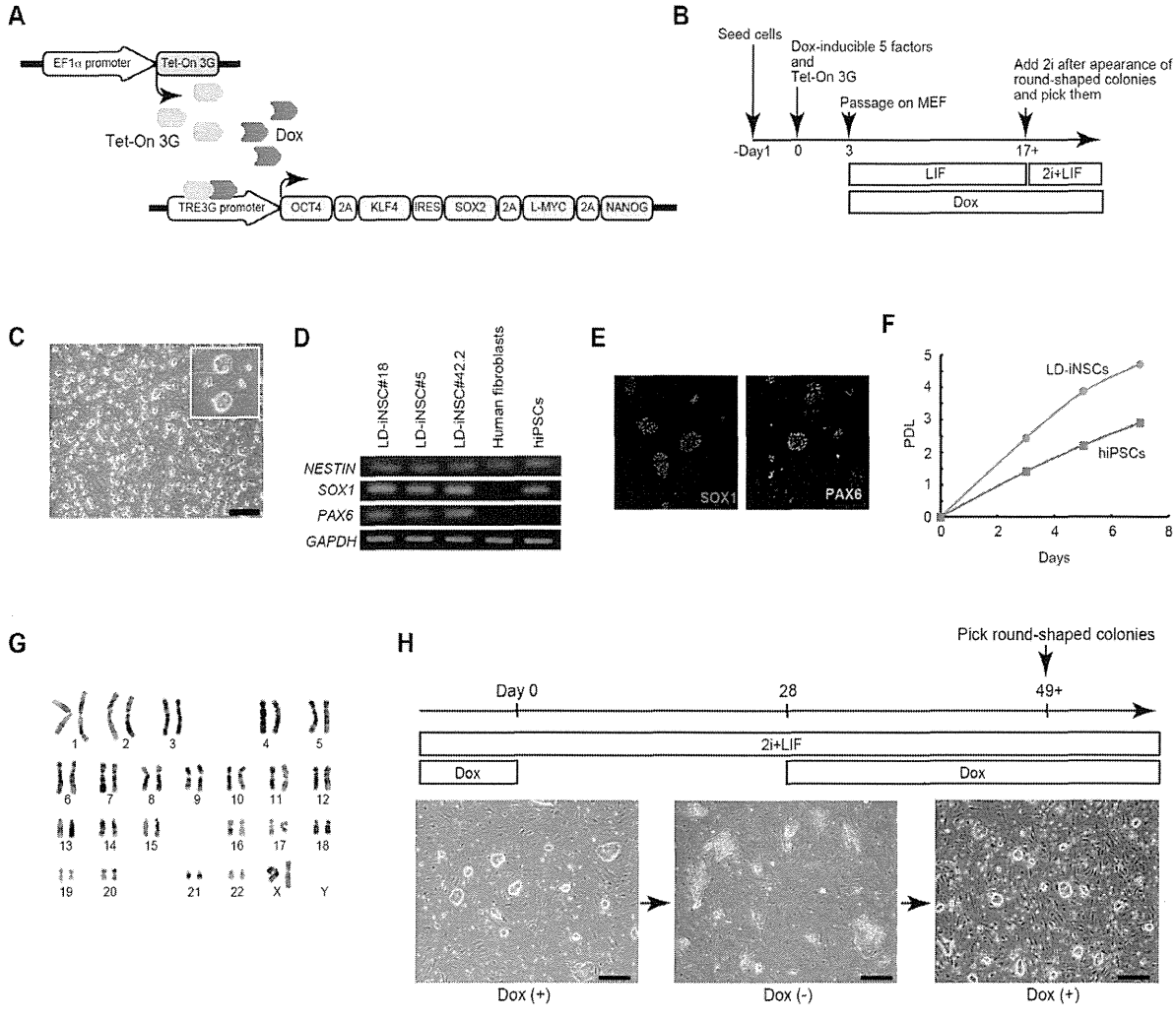

Fig. 1. Direct reprogramming of fibroblasts into LD-iNSCs. (A) Schematic representation of the doxycycline (Dox)-inducible lentiviral polycistronic vectors. The vector consists of a polycistronic gene that contains the human cDNA sequences of *OCT4*, *KLF4*, *SOX2*, *L-MYC* and *NANOG*, bound by self-cleaving 2A elements (2A) and IRES, and driven by the TRE3G promoter, which is activated by the binding of the Tet-On 3G transactivator in the presence of Dox in a culture medium. (B) Schematic of the experimental setup and strategy for the generation of LIF-dependent induced neural progenitors (LD-iNSCs). (C) Colony morphology of LD-iNSCs exhibited a tightly packed structure similar to primary neural progenitors. (D) RT-PCR showed that LD-iNSCs expressed the neural progenitor markers *NESTIN*, *SOX1* and *PAX6*. *GAPDH* was used as an internal control. RNA was extracted from three LD-iNSC clones (LD-iNSC#5, LD-iNSC#18 and LD-iNSC#42.2), uninfected parent fibroblasts (negative control), and from human iPSCs. (E) LD-iNSCs cultured on feeder cells in the presence of 2i/LIF tested positive for SOX1 (red) and PAX6 (green). (F) The population doubling level (PDL) of LD-iNSCs in comparison with human iPSCs. (G) A representative karyotype of LD-iNSCs at passage 28. (H) Ectopic factor dependence of LD-iNSCs. Upon doxycycline withdrawal, LD-iNSC colony morphology was lost, and the cells assumed a square morphology. The subsequent addition of Dox reversibly produced LD-iNSCs. Days of differentiation or reprogramming are indicated. Scale bars are 500 μm (C and H).

Biology Open (2015) 4, 1595-1607 doi:10.1242/bio.013151

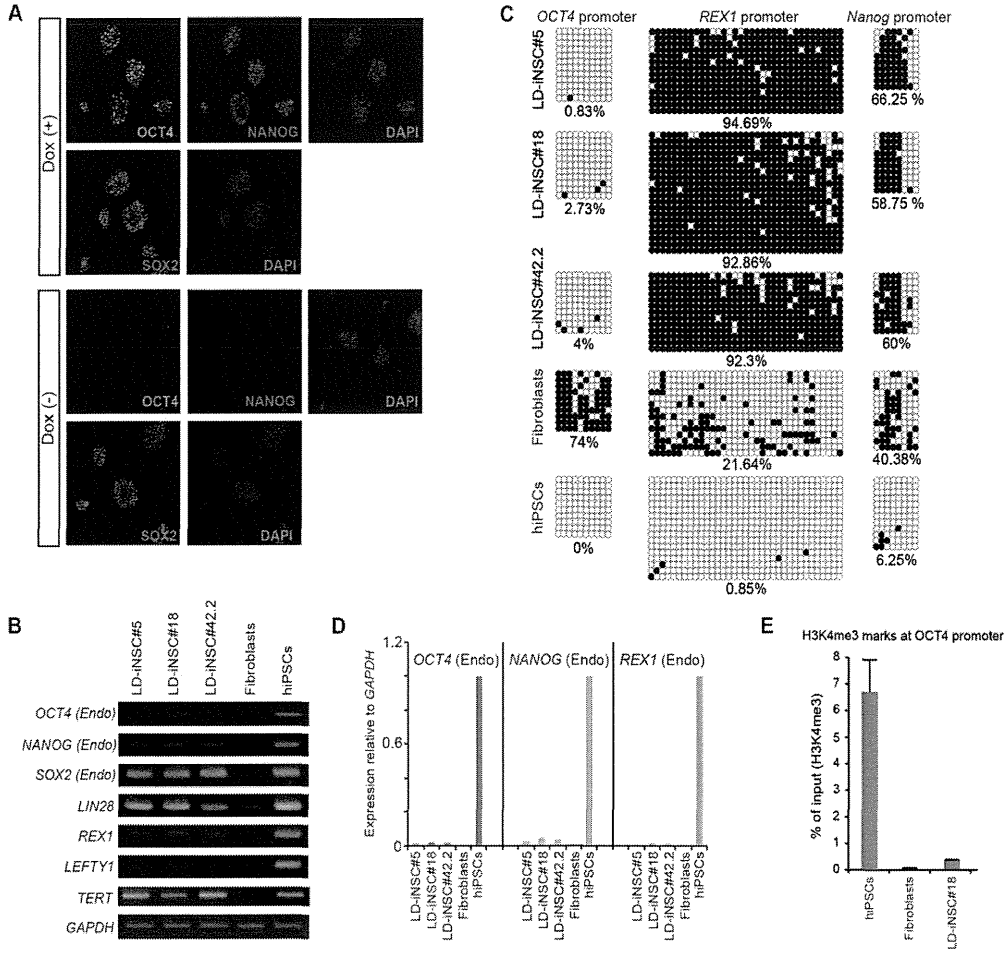

Fig. 2. Characterization of LD-iNSCs. (A) Immunostaining for OCT4, SOX2 and NANOG in LD-iNSCs with (top) or without (bottom) Dox treatment. Only SOX2 expression was detected in LD-iNSCs without Dox (bottom). Cell nuclei were visualized with DAPI. (B) RT-PCR showed that LD-iNSCs expressed markers of pluripotency, such as endogenous *OCT4*, *NANOG*, *SOX2*, *LIN28*, *REX1*, *LEFTY1* and *TERT*. *GAPDH* served as the internal control. RNA was extracted from three LD-iNSC clones (LD-iNSC#5, LD-iNSC#18 and LD-iNSC#42.2), uninfected parent fibroblasts (negative control), and from human iPSCs (positive control). (C) DNA methylation status of CpG islands in the *OCT4*, *REX1* and *NANOG* promoter regions was assessed by bisulfite sequencing PCR. Open circles indicate unmethylated, and filled circles indicate methylated, CpG dinucleotides. Representative sequences from three LD-iNSC clones (LD-iNSC#5, LD-iNSC#18 and LD-iNSC#42.2), uninfected parent fibroblasts (negative control) and human iPSCs (positive control) are shown. The percentage of CpG methylation in each CpG island within the respective cell line is indicated. (D) Expression levels of pluripotent marker genes (*OCT4*, *REX1* and *NANOG*) selected in (C). All data are normalized to hiPSCs (positive control), whose expression was assumed to be 1.0 for genes in other cell lines. (E) ChIP-qPCR analysis of the presence of histone 3 lysine 4 marker in the promoter region of the pluripotency gene *OCT4* in LD-iNSC#18, uninfected parent fibroblasts (negative control), and human iPSCs (positive control). Error bars are mean±s.e.m., n=3.

colonies were picked and maintained in the presence of LIF, Dox and 2i, which are known to promote reprogramming (Fig. 1B). These clones were expanded for further clonal analysis.

We eventually established nine individual colonies. These neuroepithelium-like cells grew as tightly packed, bright, round-shaped colonies on feeder layers (Fig. 1C), and were confirmed based on their expression of neural stem cell markers (NESTIN, SOX1 and PAX6; Fig. 1D,E, Fig. S2A). We refer to these cells as human LIF-dependent induced neural stem cells (human LD-iNSCs). Three LD-iNSC clones (#5, #18 and #42.2) were selected for further analysis. We verified the integration of copies of the lentiviral vector into the genome of these LD-iNSCs (clones #5, #18, #42.2) by Southern blotting for two independent sites in the lentiviral vector. Southern blotting confirmed that the three cell lines (#5, #18 and #42.2) were independent clones (data not shown). In addition, short tandem repeat (STR) analysis of LD-iNSCs confirmed that these cells were derivatives of the parental human fibroblasts (Table S1).

We further characterized these established LD-iNSC clones. These cells grew at a much higher proliferation rate than hiPSCs, with a doubling time of approximately 23–25 h (Fig. 1F). These cells have now been expanded for more than 100 passages in the presence of 2i/LIF/Dox, thus generating a large number of cells. Moreover, the LD-iNSC lines retained a normal karyotype (2n=46, XX; Fig. 1G) at passage 28.

Next, we tested whether growth of LD-iNSCs in the presence of 2i/LIF could reactivate the inactive X chromosome, based on previous reports that the inactive X chromosome in hiPSCs is reactivated in the presence of 2i/LIF (Hanna et al., 2010; Wang et al., 2011). However, this may be specific to the culture conditions of hiPSCs. Therefore, we analyzed the effect of 2i/LIF conditions on X inactivation in LD-iNSCs. Nonetheless, as shown in Fig. S2B and C, LD-iNSCs grown in a medium containing 2i/LIF expressed an XIST cloud in all cells, which is indicative of the continued X chromosome inactivation.

We then tested whether LD-iNSCs could be stably propagated in the absence of the five ectopic reprogramming factors (OCT4, KLF4, SOX2, L-MYC and NANOG). As shown in Fig. 1H, the withdrawal of Dox for four weeks resulted in a gradual loss of the

Biology Open (2015) 4, 1595-1607 doi:10.1242/bio.013151

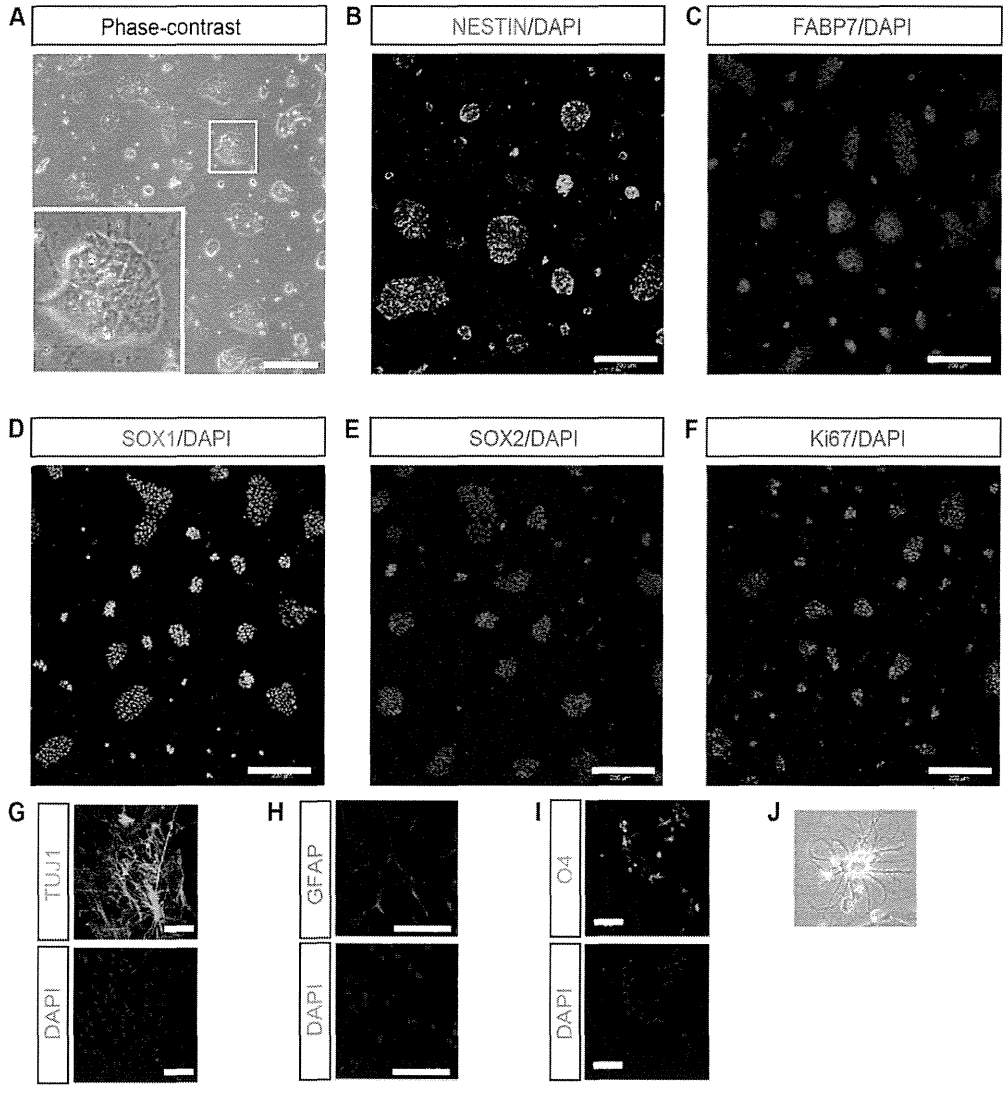

Fig. 3. Expression of neural progenitor markers in LD-iNSCs. (A) A phase-contrast image of LD-iNSCs cultured onto poly-L-lysine and laminin-coated dishes under feeder-free conditions in the presence of 2i/LIF. A high-magnification image of cells is also shown in the inset image. (B-E) LD-iNSCs without feeder cells in the presence of 2i/LIF tested positive for NESTIN (D, green), FABP7 (E, red), SOX1 (F, green) and SOX2 (G, red). DAPI staining is shown in blue. (F) Immunostaining for Ki67 (red) in LD-iNSCs without feeder cells in the presence of 2i/LIF. DAPI staining is shown in blue. (G-I) An immunofluorescence assay for the detection of markers of neurons (TUJ1), astrocytes (GFAP) and oligodendrocytes (O4). LD-iNSCs have the capacity to differentiate into neurons, astrocytes and oligodendrocytes *in vitro*. (J) Representative image of an oligodendroglial morphology. Scale bars are 200 μm (A-F) or 100 μm (G-I).

rounded NSC-like colony morphology, with all cells adopting a small flat epithelial cell-like appearance. These LD-iNSCs underwent morphological changes into neurons in response to longer-term withdrawal of Dox (Fig. S2D). This result suggested the need for some ectopic reprogramming factors for the maintenance of LD-iNSCs derived from human fibroblasts. On the other hand, round colony morphology was observed approximately three weeks after the re-addition of Dox (Fig. 1H), suggesting that LD-iNSCs depend on the expression of exogenous reprograming factors. Such strong dependence on the constitutive ectopic expression of reprograming factors during cell maintenance indicates that the LD-iNSCs were reprogrammed to a metastable state.

Characterization of LD-iNSCs

Pluripotency markers (OCT4, SOX2 and NANOG) were actively expressed in our LD-iNSCs cultured with Dox (Fig. 2A). On the other hand, when Dox was withdrawn for three days, SOX2 was detected in LD-iNSCs but neither OCT4 nor NANOG were detected (Fig. 2A). Consequently, SOX2 must have been expressed endogenously in LD-iNSCs. Other pluripotency markers in LD-iNSCs were identified by reverse transcription-polymerase chain reaction (RT-PCR). The RT-PCR analysis indicated that some of the endogenous pluripotency marker genes (*SOX2*, *LIN28* and *TERT*) were expressed at levels similar to those of hiPSCs (Fig. 2B). On the other hand, the expression of endogenous genes *OCT4*, *NANOG*, *REX1* and *LEFTY1* had been silenced in all LD-iNSC lines, in contrast to hiPSCs (Fig. 2B). Therefore, in spite of the induction by five reprogramming factors, LD-iNSCs might be multipotent stem cells and not pluripotent cells. The constitutive growth potential of LD-iNSCs was evaluated by long-term culturing of Dox-free LD-iNSCs. These cells survived regardless of the ectopic expression of reprograming factors for more than 12 weeks, and expressed *TERT*, but not endogenous *OCT4* (Fig. S3A,B). Notably, it is well known that the forced expression of *TERT* inhibits replicative senescence and extends lifespan in numerous cell types (Bodnar et al., 1998). Therefore, our results may also suggest that the expression of *TERT* extends the replicative potential of LD-iNSCs.

We then performed bisulfite-sequencing analysis in the promoter region of the pluripotency markers (*OCT4*, *NANOG* and *REX1*) to determine the levels of DNA methylation in LD-iNSCs. *NANOG* and *REX1* promoters were hypermethylated in all LD-iNSC clones, in contrast to hiPSCs. Despite the absence of *OCT4* expression in LD-iNSCs according to RT-PCR analysis (Fig. 2B), the *OCT4* promoter was unexpectedly hypomethylated in all LD-iNSC clones, in contrast to the parental somatic fibroblasts (Fig. 2C). To precisely quantitate the levels of endogenous *OCT4*, *NANOG* and *REX1* expression, we determined the level of their mRNA expression in LD-iNSCs using quantitative PCR (q-PCR). q-PCR analysis showed that LD-iNSCs failed to reactivate expression of endogenous *OCT4*, *NANOG* and *REX1* (Fig. 2D), similar to the results of the RT-PCR analysis shown in Fig. 2B. Therefore, the repression of *OCT4*

Biology Open (2015) 4, 1595-1607 doi:10.1242/bio.013151

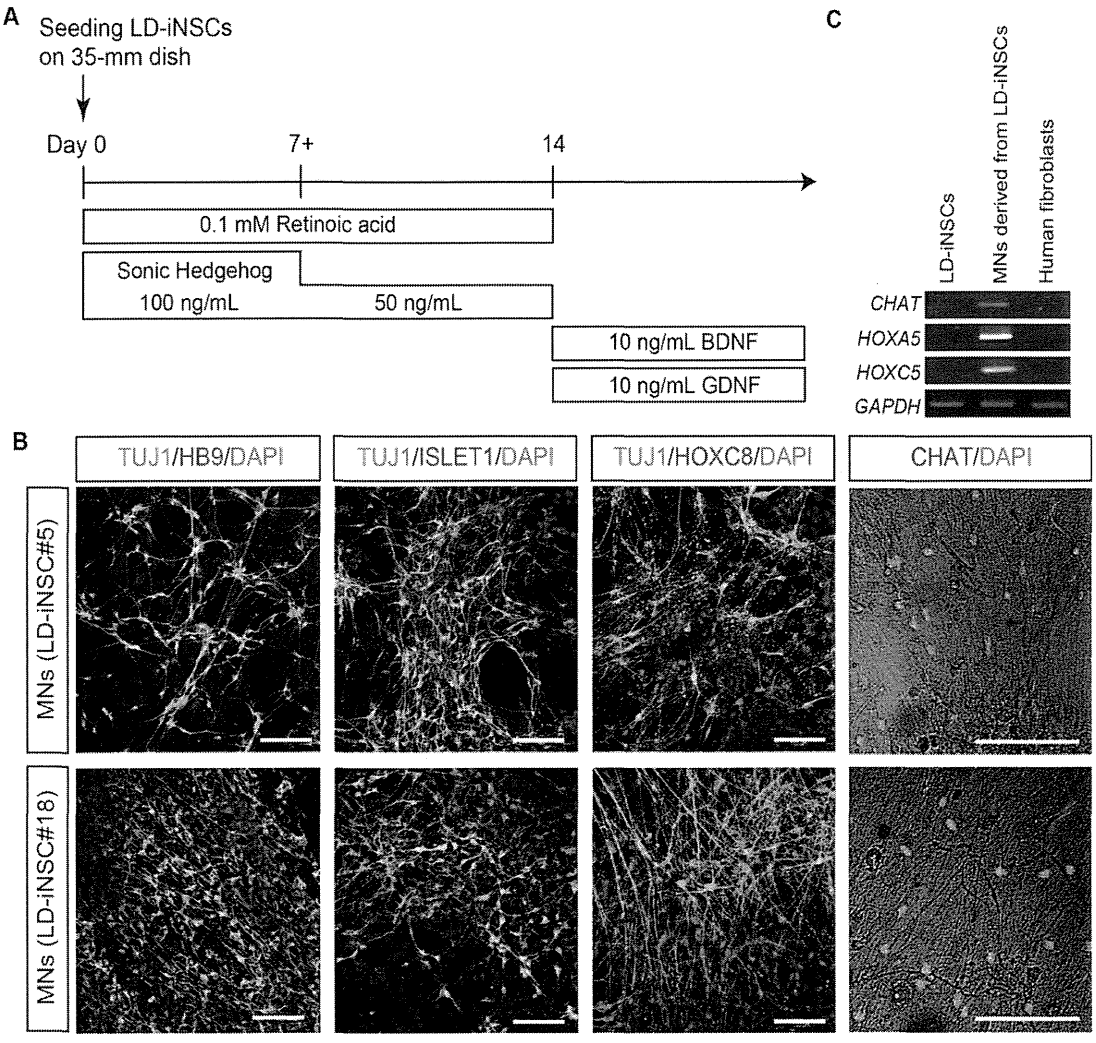

Fig. 4. Differentiation of LD-iNSC into motor neurons. (A) Schematic representation of the differentiation of LD-iNSCs into motor neurons. (B) LD-iNSC-derived motor neurons were positive for TUJ1 and expressed motor neuron markers such as HB9, ISLET1, HOXC8 and CHAT. Cell nuclei were visualized with DAPI. Scale bars are 100 µm. (C) RT-PCR revealed increased/induced expression of postmitotic markers of motor neurons (CHAT, HOXA5 and HOXC5) in LD-iNSCs-derived motor neurons in contrast to LD-iNSCs and human fibroblasts. GAPDH served as the internal control. Abbreviations: BDNF, brain-derived neurotrophic factor; GDNF, glial cell-derived neurotrophic factor.

expression in LD-iNSCs was not strongly linked to gene silencing, resulting from the methylation of the *OCT4* promoter region. Therefore, to verify the histone modification state in the *OCT4* promoter region, we determined the presence of activating histone markers in the *OCT4* promoter region, which are also known to be regulators of pluripotency (Bernstein et al., 2006). We analyzed the presence of the activating histone marker, histone 3 lysine 4-trimethylation (H3K4me3), in the *OCT4* promoter region using chromatin immunoprecipitation (ChIP) and q-PCR. H3K4me3 enrichment was observed in the *OCT4* promoter region of hiPSCs, but not in LD-iNSC#18 (Fig. 2E). These results suggested that the suppression of *OCT4* mRNA expression in LD-iNSCs was caused by a low level of transcriptionally active H3K4 methylation markers in the *OCT4* promoter region. However, reduced H3K4me3 deposition at active promoters in stem cells does not drastically affect steady-state transcription (Clouaire et al., 2012; Jiang et al., 2011). Therefore, *OCT4* expression in LD-iNSCs might also be regulated by other epigenetic mechanisms and transcription factors.

LD-iNSCs display characteristics of primitive neural stem cells

We next tested if the LD-iNSCs possessed the characteristics of primitive human NSCs (hNSCs). LD-iNSCs were grown without a feeder layer in the presence of 2i/LIF/Dox in order to verify their morphology. As shown in Fig. 3A, LD-iNSCs displayed a dome-shaped morphology, consistent with previous findings (Theunissen et al., 2014). Immunofluorescence analysis also indicated the expression of NSC markers, including NESTIN, SOX1, SOX2 and FABP7 (Fig. 3B-E). In addition, the LD-iNSCs were highly proliferative, as evidenced by the expression of Ki67 in a majority of the cells (Fig. 3F, Fig. S4A).

Recently, neural stem/progenitor cells have been directly generated from primate fibroblasts by inducing with Yamanaka factors in a chemically defined medium containing LIF, GSK3 inhibitor (CH), and the transforming growth factor (TGF)-β inhibitor SB431542 (SB) (Lu et al., 2013). It is also known that this unique combination of CH, SB and LIF is required for long-term self-renewal of primitive NSCs in a chemically defined culture medium (Li et al., 2011). Therefore, we tested if LD-iNSCs could also grow in the presence of CH/SB/LIF, as well as 2i/LIF. As shown in Fig. S4B, LD-iNSCs showed long-term self-renewal when passaged serially on Matrigel with CH, SB and LIF. We further attempted to confirm the multipotency of LD-iNSCs by evaluating their ability to differentiate into neurons, astrocytes and oligodendrocytes. Immunostaining revealed the appearance of TUJ1-positive neurons, GFAP-positive astrocytes and O4-positive

Biology Open (2015) 4, 1595-1607 doi:10.1242/bio.013151

oligodendrocytes (Fig. 3G-J). Likewise, LD-iNSCs generated from BJ foreskin fibroblasts also displayed the ability to differentiate into a lineage of neurons and glia (Fig. S4C), suggesting that LD-iNSCs are indeed multipotent NSCs.

LD-iNSCs differentiate into neurons *in vitro*

The above observations suggest that *in vitro*-expanded LD-iNSCs may possess an identity similar to primitive NSCs. We further tested if LD-iNSCs, like NSCs, can differentiate into a specific neuronal subtype. We first confirmed that LD-iNSCs could differentiate into motor neurons. Under the differentiation conditions shown in Fig. 4A, all LD-iNSC clones (#5, #18 and #42.2) expressed pan-neuronal markers, such as TUJ1; these TUJ1-positive neurons also expressed post-mitotic lineage-specific markers of motor neurons, such as homeobox genes *HB9*, *ISLET1* and *HOXC8*, and the choline acetyltransferase neurotransmitter, *CHAT* (Fig. 4B and Fig. S4D). Motor neuron identity was also confirmed at the transcriptional level by RT-PCR (Fig. 4C). Accordingly, these results indicated that our TUJ1-positive neurons had the properties of mature motor neurons. Thus, LD-iNSCs efficiently differentiated into postmitotic motor neurons via simple induction with sonic hedgehog (SHH) and retinoic acid (RA).

We next tested if LD-iNSCs also have the capacity to differentiate into other neuronal subtypes such as dopaminergic (DA) neurons. The DA neuron differentiation conditions shown in Fig. 5A induced the differentiation of LD-iNSCs into neurons exhibiting EN-1, LMX1A, NURR1 and FOXA2 immunoreactivity (Fig. 5B-E). In addition, these transcription factor genes, encoding for mesencephalic DA neuron markers, were expressed in most of the TUJ1-positive neurons. Tyrosine hydroxylase (TH) was also present in the differentiated LD-iNSCs, suggesting that these cells differentiated into mature dopaminergic neurons. To determine the properties of the LD-iNSCs, we measured the number of DA neurons differentiated from LD-iNSCs and hESC-derived NSCs (n=6). The LD-iNSCs yielded a higher proportion of TH+/TUJ1+ DA neurons (21.2±6.7%) than NSCs (negligible) (Fig. 5G). These results indicate that LD-iNSCs have significantly greater potency than hESC-derived NSCs in generating DA neurons.

Conversion of LD-iNSCs into conventional hiPSCs

Geijsen and colleagues have previously reported that the ability of self-renewal in hLR5 cells is dependent on the expression of ectopic reprogramming factors (OCT4, SOX2, KLF4, c-MYC and NANOG), similar to the LD-iNSCs of this study (Buecker et al., 2010). On the other hand, we do not know if hLR5 cells have the same properties as neural stem/progenitor cells. hLR5 cells can be converted to a stable, epiblast-like pluripotent state by simultaneously removing the ectopic reprogramming factors and altering the culture growth factor conditions. Therefore, we attempted to verify if changes in the growth factor environment could induce a similar conversion of LD-iNSCs to a stable pluripotent state (conventional hiPSCs).

Fig. 6A shows the timeline of conversion of LD-iNSCs to conventional hiPSCs. Initially, LD-iNSCs dissociated by trypsinization were plated on feeder cells (density: 1.5×10^5 cells/100-mm dish) in a medium containing 2i/LIF/Dox. The medium containing 2i/LIF/Dox was switched to hESC medium supplemented with bFGF (Fig. 6A) on day 2. Most colonies of

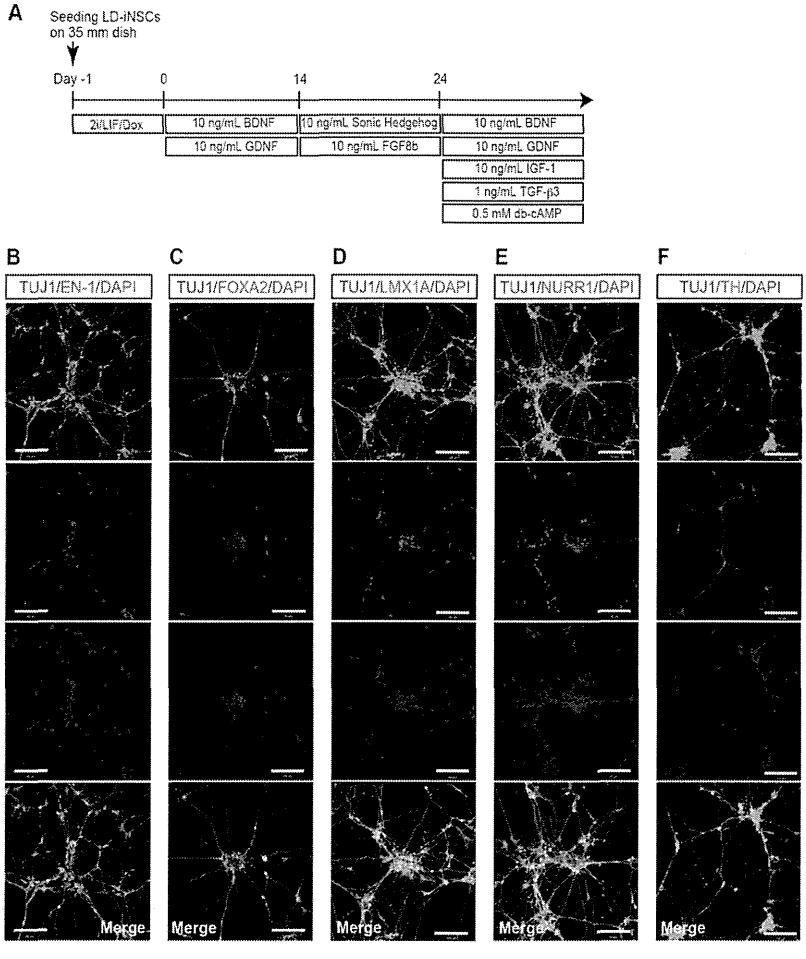

Fig. 5. Differentiation of LD-iNSCs into dopaminergic neurons. (A) An overview of the protocol for differentiation of LD-iNSCs into dopaminergic neurons. (B-F) Efficient production of dopaminergic neurons from LD-iNSCs was demonstrated by immunostaining for EN-1, FOXA2, LMX1A, NURR1 and TH (red). TUJ1 is a pan-neuronal marker used to assess the total production of neurons (green). Cell nuclei were visualized with DAPI. Scale bars are 100 μm (B-F). Abbreviations: FGF8b, fibroblast growth factor 8 b; IGF-1, insulin-like growth factor-I; TGF-β3, transforming growth factor beta 3; db-cAMP, dibutyryl cyclic adenosine monophosphate. (G) Percentage of TH+ neurons among total neurons (TUJ1+) differentiated from LD-iNSCs and hESC-derived NSCs under DA neuronal differentiation conditions was determined by immunofluorescence. Error bars are mean±s.e.m., n=6.

Biology Open (2015) 4, 1595-1607 doi:10.1242/bio.013151

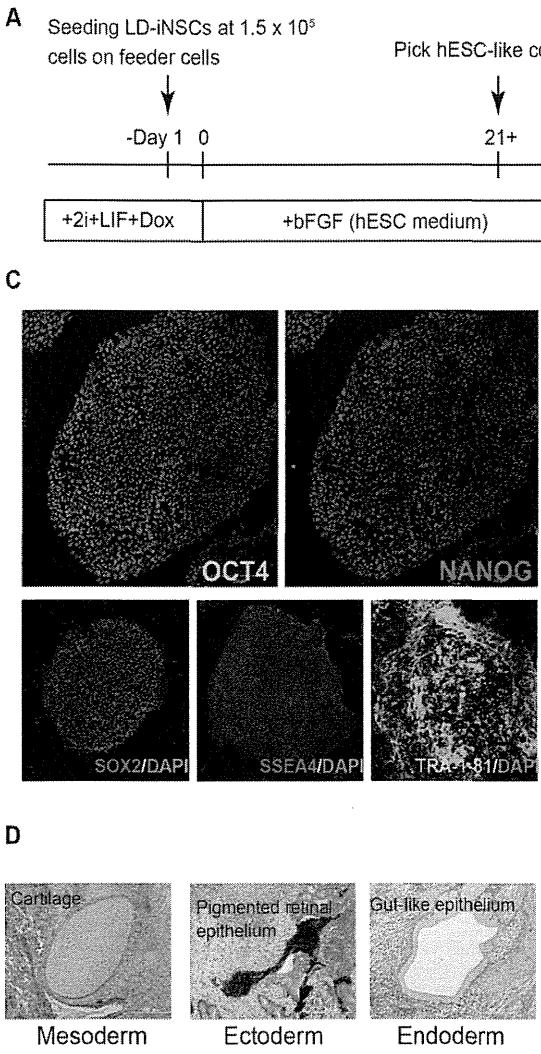

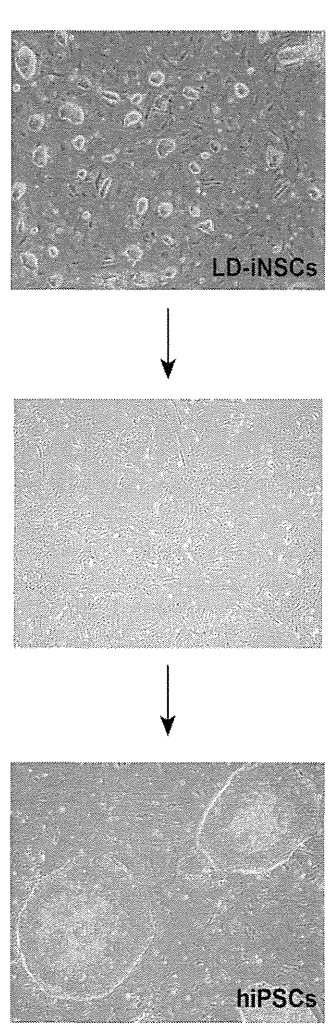

Fig. 6. Conversion of LD-iNSCs to hiPSCs. (A) Schematic representation of the conversion of LD-iNSCs to a stable pluripotent state. (B) Three days after switching to the standard hESC medium supplemented with bFGF, LD-iNSC lost its colony morphology (top panel) and the cells adopted a fibroblast-like appearance (middle panel). After further growth in this culture condition, LD-iNSCs were converted to hiPSCs (bottom panel). The converted cells (LD5F-hiPSCs) exhibited hESC-like colony morphology. (C) Typical ESC markers (OCT4, NANOG and SOX2) were expressed in LD5-hiPSCs, according to immunofluorescence analysis. Other pluripotent cell surface markers (SSEA4 and TRA-1-81) were also detected by immunofluorescence staining. DAPI was used to visualize the cell nuclei. (D) Injection of undifferentiated LD5F-hiPSCs into immune-deficient mice led to the formation of teratomas containing derivatives of all three germ layers: cartilage (mesoderm, left panel), pigmented retinal epithelium (ectoderm, middle panel) and gut-like epithelium (endoderm, right panel).

LD-iNSCs immediately broke up after downregulation of the ectopic reprogramming factors (Fig. 6B). Nonetheless, hESC-like colonies emerged on or after day 21, and were mechanically picked for expansion. These colonies eventually displayed a typical hiPSC-like morphology (Fig. 6B). These were therefore referred to as LD-iNSC-derived 5-factor hiPSCs (LD5F-hiPSCs). The conversion frequency of LD-iNSCs into LD5F-hiPSCs was approximately 0.01%, similar to the conversion of hLR5 cells into hiPSCs (Buecker et al., 2010). In order to confirm that the LD5F-hiPSCs (clones #55 and #57) were indeed derived from LD-iNSC #18, we analyzed the clones by Southern blotting for two independent sites in the lentivirus vector, which was randomly integrated into the genome of these cells. The Southern blot revealed that the distribution of all lentiviral vector integration sites in LD5F-hiPSCs was identical to the pattern of the parental LD-iNSC clone #18 (data not shown). Therefore, these results confirmed that LD5F-hiPSCs (clones #55 and #57) were derived from LD-iNSC clone #18. The resulting LD5F-hiPSCs displayed typical hESC morphology, and were subsequently maintained with bFGF alone, indicating that LD5F-hiPSCs need not be activated by the LIF signaling pathway.

To further characterize the LD5F-hiPSC phenotype, we performed a comprehensive molecular analysis at the protein level. Immunostaining revealed that LD5F-hiPSCs consistently expressed numerous pluripotency markers, including OCT4, SOX2, NANOG, SSEA4 and TRA-1-81 (Fig. 6C). We also attempted to verify if the LD5F-hiPSCs acquired pluripotency by subcutaneously injecting LD5F-hiPSCs into immunosuppressed mice; the resulting tumors were enucleated after 10 weeks. Histological analysis revealed the presence of teratomas containing tissues of all three germ layers, including the cartilage (mesoderm), pigmented retinal epithelium (ectoderm) and gut-like epithelium (endoderm; Fig. 6D). These results indicated that LD5F-hiPSCs had the ability to proliferate indefinitely (without commitment to any cell lineage regardless of the ectopic reprogramming factors) and the capacity to differentiate into cell lineages from the three germ layers. In addition, LD-iNSCs were more amenable to the introduction of transgenes than hiPSCs (Fig. 7A,B), suggesting that LD-iNSCs can be useful in research and the development of novel cell therapies for neurodegenerative diseases.

DISCUSSION

In this study, we investigated a strategy for the generation of multipotent stem cells (LD-iNSCs) with NSC properties from human fibroblasts using five reprogramming factors (OCT4, KLF4, SOX2, L-MYC and NANOG). The efficiency of LD-iNSC generation from fibroblasts was approximately 0.01–0.03%, as determined from the initial number of fibroblasts (1.5×10^5) used in the reprogramming experiments. These LD-iNSCs showed self-renewal capacity in the presence of LIF and inhibitors of GSK3β and ERK1/2 signaling, and five ectopic reprogramming genes. The expanded LD-iNSCs are capable of differentiating into neurons, astrocytes and oligodendrocytes, suggesting that LD-iNSCs have the predictable identity of LIF-dependent primitive NSCs (Fig. 8A).

Biology Open (2015) 4, 1595-1607 doi:10.1242/bio.013151

In general, mouse primitive NSCs (LIF dependent, but independent of exogenous bFGF) can be derived from mESCs *in vitro* or from the epiblast [embryonic day 5.5 (E5.5) to E7.5] and the neuroectoderm (E7.5–E8.5) *in vivo* (Tropepe et al., 2001). Definitive NSCs (LIF independent and bFGF dependent) first appear in the E8.5 neural plate and persist for life (Wada et al., 2006). Therefore, LIF-dependent primitive NSCs give rise to definitive NSCs (Hitoshi et al., 2004), suggesting that primitive NSCs have a higher neurogenic potential than definitive NSCs. Therefore, this indicated that LD-iNSCs are capable of differentiating into bFGF-dependent definitive NSCs. However, the replacement of 2i/LIF medium with neural stem cell medium supplemented with bFGF and EGF led to a majority of the cells losing their NSC-like ability, and thereby could not be cultured for more than one month. LIF functions as a survival factor for primitive NSCs (Smukler et al., 2006). Therefore, when LIF is removed from the primitive NSC culture system to induce bFGF-dependent definitive NSCs, the passage of primitive NSCs to definitive NSCs may result in significant cell death. On the other hand, once a population of definitive NSCs is established after LIF withdrawal, these cells can propagated in NSC culture medium supplemented with bFGF. Therefore, this initial adaptation to cell culture conditions may be important for the prevention of cell death. The establishment and long-term maintenance of primitive hNSCs from embryonic, fetal, newborn, and adult tissues is a difficult task; there are also limitations on the number of graft materials that can be used for primitive hNSCs. Primitive hNSCs can also be derived from hESCs/iPSCs; however, chemically defined conditions for the long-term maintenance of primitive hNSCs are unknown (Li et al., 2011). Therefore, the induction of primitive hNSCs from hESCs/iPSCs may result in ineffective generation of hNSCs or retention of hESC/iPSC characteristics. This increases the risk of development of immature teratomas following the transplantation of iPSC-derived multipotent stem cells or their progeny, as a result of possible iPSC contamination or incomplete reprogramming. This suggests that there are several limitations to the use of iPSCs in neural cell-based therapy or in neural disease modeling.

In general, reprogramming factors such as the Yamanaka factors are used to drive somatic cells into a pluripotent state. Kim et al. (2011) showed that mouse fibroblasts are converted to neural stem cells by bypassing the iPSC stage with help from the same factors. Therefore, our study might also support the hypothesis that neural stem cells can be derived during the iPSC induction process.

Unexpectedly, LD-iNSC colonies appeared approximately after day 14 in this study, whereas the iPSC colonies were not observed for 3–4 weeks after viral infection in the presence of 2i/LIF and Dox. These data suggest that LD-iNSCs are most likely generated via direct conversion from fibroblasts rather than through rapid differentiation from iPSCs into primitive NSCs. Our LD-iNSCs were reprogrammed into a stable pluripotent state when the culture medium was changed to hESC medium supplemented with bFGF (Fig. 8A). This finding indicates that LD-iNSCs are derived from intermediate, partially reprogrammed cells. Further characterization of LD-iNSCs showed that the pluripotency genes – *OCT4*, *NANOG* and *REX1* – was not significantly activated during this process. The

A

Introduction efficiency of transgenes into LD-iNSCs and hiPSCs by electroporation (Neon)

Cell Type	Plasmid	Transfection Efficiency
LD-iNSCs	CAG-EGFP (15 kb)	~50%
hiPSCs	CAG-EGFP (15Kb)	0%

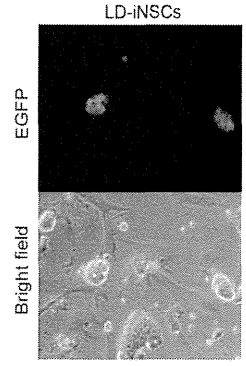

B

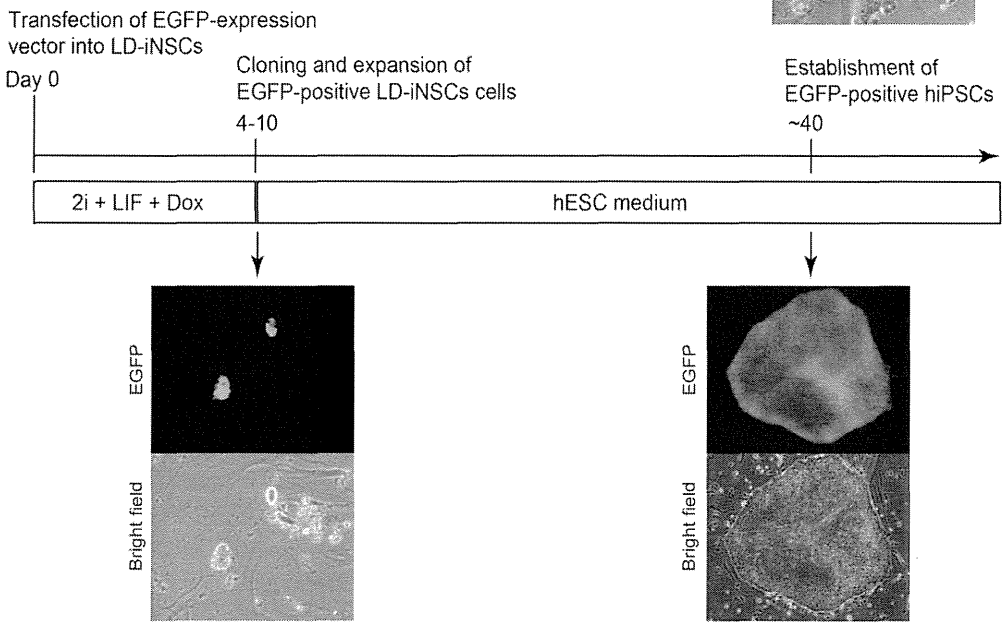

Fig. 7. Introduction of a transgene into LD-iNSCs. (A) Results of the electroporation experiments with LD-NPs and hiPSCs are summarized in the table (left panel). The right panel shows representative images of LD-iNSCs after electroporation of an EGFP expression vector (15 kb). As shown in the table, the percentage of EGFP-positive LD-iNSC colonies was approximately 50% under our transfection conditions, but negligible or 0% in conventional hiPSCs. (B) Conversion of EGFP-positive LD-iNSCs to a stable pluripotent state. hiPSCs converted from an EGFP-positive LD-iNSC clone were obtained at the indicated time point. mESCs/iPSCs have generally demonstrated a relatively high level of transfection efficiency, whereas hESCs/iPSCs are notoriously difficult to transfect (Cao et al., 2010). Therefore, these results suggest that the conversion to hiPSCs might be a novel method that could increase the transfection efficiency of hiPSCs.

Biology Open (2015) 4, 1595-1607 doi:10.1242/bio.013151

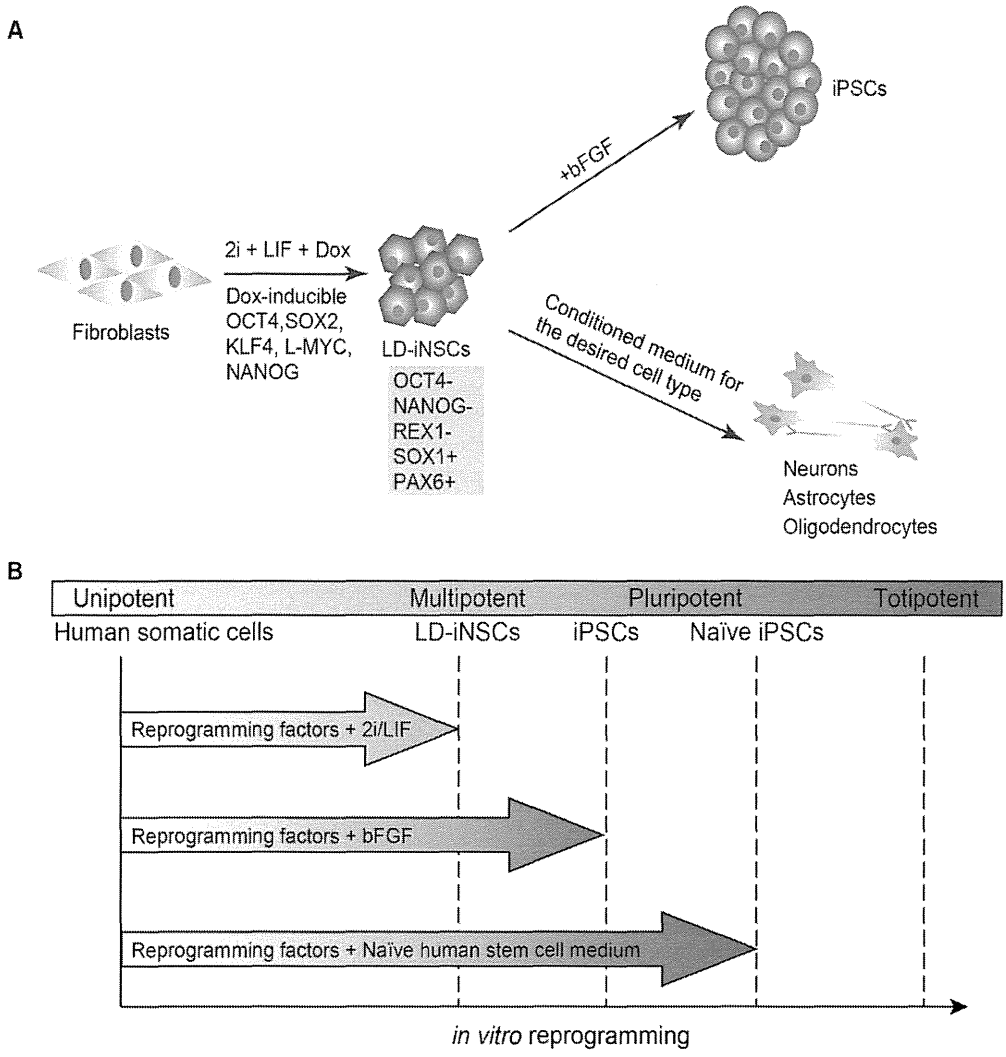

Fig. 8. LIF-dependent primitive NSCs are obtained in the process of reprogramming to iPSCs. (A) The establishment of various desired neuronal types by means of multipotent LD-iNSCs. LD-iNSCs are directly derived from human fibroblasts via continuous expression of reprogramming factors in the presence of 2i/LIF in the culture medium. LD-iNSCs retain low levels of OCT4 and NANOG expression, but high levels of SOX2 expression, have self-renewal capacity, and can differentiate into various neuronal types (such as motor neurons and dopaminergic neurons), astrocytes and oligodendrocytes. In addition, pluripotent stem cells can be derived by simple re-plating of LD-iNSCs in hESC medium supplemented with bFGF, suggesting that LD-iNSCs are derived from intermediate partially reprogrammed cells. (B) Pluripotency levels induced by *in vitro* reprogramming correlate significantly with the extrinsic signaling environment. The delivery of reprogramming factors into primary human fibroblasts, and culturing of the cells in the presence of 2i/LIF leads to the resulting cell lines (such as LD-iNSCs) resembling multipotent primitive neural stem/progenitor cells (Hirano et al., 2012). Aside from the 2i/LIF treatment, bFGF signaling plays an important role in the derivation and maintenance of hiPSCs (a primed state). Fully naïve hiPSCs were recently derived using a novel medium called naïve human stem cell medium (NHSM) (Gafni et al., 2013). Taken together, the combination of reprogramming factors and culture supplements determines the respective pluripotent states.

silenced status of these genes was also confirmed by epigenetic changes in the promoter regions of the relevant pluripotency regulators. The *NANOG* and *REX1* promoter regions were hypermethylated in LD-iNSCs. Unexpectedly, the methylation level in the *OCT4* promoter region in LD-iNSCs was the same as that in hiPSCs. Similarly, the methylation status of the *OCT4* promoter in LIF-dependent primitive NSCs is also low, similar to ESCs (Akamatsu et al., 2009). Therefore, *OCT4* silencing in LD-iNSCs might be attributed to a decrease in the level of the transcriptionally active H3K4 methylation marker, than the promoter methylation status. Hypomethylation of the *OCT4* promoter region indicates that LD-iNSCs are in a state that is poised towards pluripotency. Therefore, the fact that LD-iNSCs are partially reprogrammed intermediate cells could also be explained in terms of the epigenetic status. However, cultivation of stem cells in the presence of 2i (two small molecules: CHIR99021 and PD0325901) and LIF can induce a naïve state in mouse pluripotent stem cells (Hanna et al., 2009; Ying et al., 2008). Moreover, several groups recently generated mESC-like hiPSCs by applying the naïve culture conditions after inducing with reprogramming factors; however, such cell lines lack the phenotypic stability that distinguishes bona fide mESCs/iPSCs (Hanna et al., 2010; Li et al., 2009). In this study, we did not detect the expression of pluripotency markers in several of the hiPSC lines when cultivating the cells in the presence of 2i and LIF, and absence of reprogramming factors. Moreover, none of the examined hiPSC lines differentiated into LIF-dependent primitive neural progenitors in the presence of 2i/LIF alone. This result indicates that the ectopic expression of specific reprogramming factors is essential for the self-renewal of LD-iNSCs. This finding is consistent with those of a previous report, wherein the exogenous reprograming factors were shown to be reactivated in primitive NSCs derived from hiPSCs in the presence of 2i/LIF (Hirano et al., 2012). Similarly, recent publications also suggest that the stability of transdifferentiated phenotypes appears to depend on the sustained overexpression of reprogramming transgenes (Ieda et al., 2010; Sheng et al., 2012). Li